Journal of Geochemical Exploration 111 (2011) 113–137

Contents lists available at ScienceDirect

Journal of Geochemical Exploration

journal homepage: www.elsevier.com/locate/jgeoexp

Provenance, tectonics and source weathering of modern fluvial sediments of the Brahmaputra–Jamuna River, Bangladesh: Inference from geochemistry

Mohammad Amir Hossain Bhuiyan [a,b,*], M. Julleh Jalalur Rahman [c], Samuel B. Dampare [a], Shigeyuki Suzuki [a]

[a] Department of Earth Sciences, Okayama University, 1-1, Tsushima-Naka, 3Chome, Okayama 700-8530, Japan
[b] Department of Environmental Sciences, Jahangirnagar University, Dhaka 1342, Bangladesh
[c] Department of Geological Sciences, Jahangirnagar University, Savar, Dhaka-1342, Bangladesh

ARTICLE INFO

Article history:
Received 17 August 2010
Accepted 29 June 2011
Available online 31 July 2011

Keywords:
Geochemistry
Fluvial sediments
Provenance
Weathering
Brahmaputra–Jamuna River
Chemical index of alteration

ABSTRACT

This present study describes the elemental geochemistry of fluvial sediments in the Kurigram (upstream) to Sirajganj–Tangail (downstream) section of the Brahmaputra–Jamuna River, Bangladesh, with the aim of evaluating their provenance, weathering and tectonic setting. Petrographically, the sediments are rich in quartz (68%), followed by feldspars (8.5%) and lithic grains (7%). The bulk sediment chemistry is influenced by grain size. Concentrations of TiO_2, Fe_2O_3, MgO, K_2O, P_2O_5, Rb, Nb, Cr, V, Y, and, Ce, Th and Ga slightly decrease with increasing SiO_2/Al_2O_3 and grain size, suggesting clay matrix control. In contrast, concentrations of CaO, Na_2O, Sr and Pb increase with increasing SiO_2/Al_2O_3 and grain size, suggesting residence of these substances in feldspar. Decrease in Zr as grain size increases is likely controlled both by clay matrix and heavy minerals. In addition, heavy minerals' sorting also influences Ce, Th, Y and Cr abundances in some samples. The sediments are predominantly quartzose in composition with abundant low-grade metamorphic and sedimentary lithics, low feldspars and trace volcanic detritus, indicating a quartzose recycled orogen province as a source of the sediments. Discriminant diagrams together with immobile element ratio plots show that, the Brahmaputra–Jamuna River sediments are mostly derived from rocks formed in an active continental margin. Moreover, the rare earth element ratios as well as chondrite-normalized REE patterns with flat HREE, LREE enrichment, and negative Eu anomalies indicate derivation of the sediments of Brahmaputra–Jamuna River from felsic rock sources of upper continental crust (UCC). The chemical indices of alteration suggest that Brahmaputra–Jamuna River sediments are chemically immature and experienced low chemical weathering effects. In the A–CN–K ternary diagram, most of the samples close to the plagioclase–K-feldspar join line and to the UCC plot, and in the field of various lithologies of Higher Himalayan Crystalline Series, suggesting that rocks in these series are likely source rocks. Therefore, the elemental geochemistry of the Brahmaputra–Jamuna River sediments is controlled mostly by mechanical breakdown of lithic fragments and subsequent preferential attrition of muscovite>albite>quartz.

1. Introduction

The geochemical records of clastic sediments represent an archive for studying their provenance as well as the tectonics and weathering conditions in their source region (e.g., Bhatia, 1983; Cullers, 1988; Fedo, et al., 1996; Feng and Kerrich, 1990; Garver and Scott, 1995; Holail and Moghazi, 1998; McCann, 1998; McLennan and Taylor, 1983; Nesbitt and Young, 1996; Singh and Rajamani, 2001a,b; Wronkiewicz and Condie, 1987). For example, immobile major and trace elements, such as Al, Fe, Ti, Th, Sc, Co, Zr, and rare earth elements (REEs) predominantly carried in the particulate load of rivers are useful indicators of the source of sediments/sedimentary rocks (Taylor and McLennan, 1985). These elements are capable of revealing also the nature of weathering at the source region of sediments, which, in turn, is controlled by climatic and tectonic factors. The relevance of immobile elements in studying the provenance of fluvial sediments is based on the hypothesis that they experience little geochemical fractionation during weathering. Immobile elements and REEs are generally concentrated in fine-grained sediments because their host minerals together with accessory primary minerals and secondary minerals occur in that size range. Hence, the geochemistry of sediments is useful in deducing the provenance as well as climate and tectonics of the catchment region (Singh, 2009).

Major rivers of the world have been investigated by several geochemists for their continental materials (Singh et al., 2005 and references therein). Sarin et al. (1989) studied major ion chemistry of the Ganges–Brahmaputra river system to understand weathering processes of the region and elemental fluxes of the rivers to the Bay of Bengal (BoB). Singh et al. (2005) conducted a study about weathering in

* Corresponding author at: Department of Earth Sciences, Okayama University, 1-1, Tsushima-Naka, 3Chome, Okayama 700-8530, Japan. Tel.: +81 86 251 7881; fax: +81 86 251 7895.
E-mail address: amirhb75@yahoo.com (M.A.H. Bhuiyan).

0375-6742/$ – see front matter © 2011 Elsevier B.V. All rights reserved.
doi:10.1016/j.gexplo.2011.06.008

the Ganga alluvial plain based on fluvial geochemistry of the Gomati River. Galy and France-Lanord (2001) estimated that the total erosion flux from the Himalaya is two-fold of estimated suspended load fluxes in Bangladesh. This implies that the sediments transported by the Himalayan Rivers (HR) have variable residence periods on land. It is noteworthy that the HR in general and the Ganges River (GR) in particular, travel long distances along hilly tracts and plains before meeting the sea. More recently, Singh (2010) carried out a study on geochemistry and provenance of stream sediments of the GR and its major tributaries in the Himalayan region, India. Besides, Borges et al. (2008) evaluated the provenance and weathering control on river bed sediments of the eastern Tibetan Plateau and the Russian Far East. France-Lanord et al. (1993) worked on the evolution of the Himalaya since Miocene, using isotopic and sedimentologic evidence from the Bengal Fan. Rahman and Faupl (2003) worked on the composition of subsurface Neogene shales of the Surma Group in the Sylhet Trough, Bengal Basin (BB), Bangladesh, in relation to the Asia–Greater India collision and the evolution of the eastern BoB. Recently, Rahman and Suzuki (2007) employed geochemistry to evaluate the provenance, tectonic setting and weathering control of sandstones in the Miocene Surma Group in the BB. Furthermore, Rahman et al. (2008) studied the geochemistry of Neogene sandstones and recent beach sands in the Inani–Dakhin Nhila area of Bengal east coast. To date, the fluvial geochemistry of the major rivers in BB is far from the adequate attention of scientific community.

The focus of the present study is the Brahmaputra–Jamuna River (BJR), which is a sandy braided fluvial system with enormous terraced flood plains of different ages in the central and lower reaches (Fig. 1). The BJR has been receiving sediments from the Himalayas, a tectonically active highland, at least from the Cenozoic to the present time (Dewey and Bird, 1970; France-Lanord et al., 1993; Hodges, 2000). After the continental collision between India and Asia at ca. 54 Ma (Dewey et al., 1989; Harrison et al., 1992; Molnar and Tapponnier, 1975; Tapponnier et al., 1986), the Himalayan belt experienced intense folding and erosion whereby huge quantities of terrigenous detritus were released from source rocks and then deposited in primordial and recent foreland basins (Das et al., 2006). The sedimentary deposits in these basins consist primarily of terrigenous materials eroded from the orogenic belt and, thus, provide evidence for the unroofing history of the orogen, the patterns of tectonics, and the nature of sediment dispersal from the source region to the depositional environment.

The BJR floodplain encompasses vicinities that have varied topography and climate. The sediments transported and deposited by the BJR have different residence periods in various parts of the river system and have experienced different climate regimes, such as from cold and frigid in the highlands to humid and sub-tropical in the floodplains. Thus, fluvial sediments in the BJR provide an opportunity to gain knowledge about the influence of en-route climate change and other different processes on sediment chemistry. This knowledge has significant implication for the use of sediment chemistry as a proxy in the interpretation of ancient climate in the source region of fluvial sediments.

The present study was, therefore, designed to explore the geochemistry of the BJR fluvial sediments and evaluate the differences between the bar-top and different facies units for provenance, tectonics and weathering implications.

2. Geology and geomorphologic setting

The Brahmaputra River (BR), which emerges from the Tibetan Himalaya (TH), was formed as a result of linking of numerous prominent

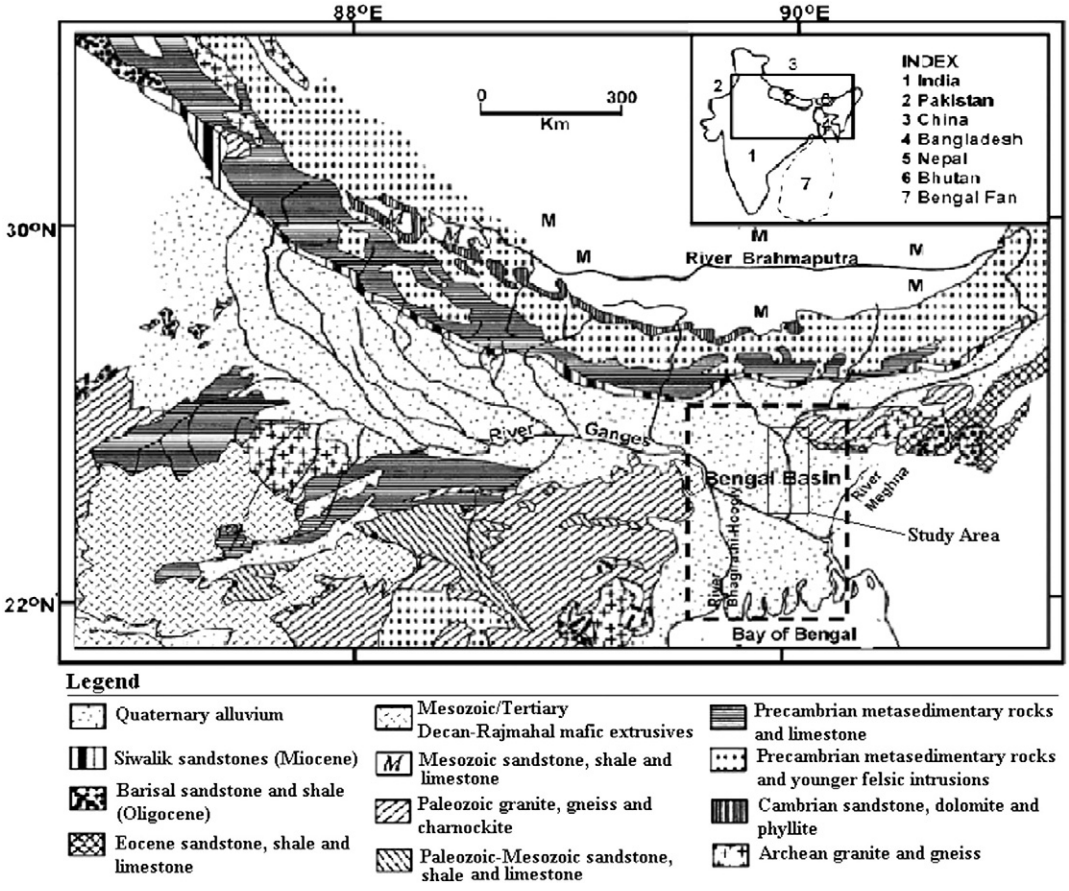

Fig. 1. Regional geology and location map of the study area (modified after Mukherjee et al., 2009).

tributaries, including the eastern drainage systems namely the Bhagirathi, Alaknanda and Mandakini which travel along the Indus Tsungpo Suture through rocks of the Higher Himalayan Crystalline Series (HHCS), Lesser Himalayas Series (LHS) and the Shillong Plateau (Fig. 2). These rivers, tributaries and drainage systems have different altitudes and reliefs. The Higher Himalayas, from which the major rivers and tributaries originate, are snow-capped most of the time and has tremendously rugged topography. The gradients of rivers in the eastern and central parts of the Eastern Himalayas are very high, with elevations, from as high as ca.5000 m to as low as 1000 m. Drainage tributaries meet at different places in this province, but eventually shape the main stream of the sandy braided BR at Assam, which finally enters Bangladesh at Kurigram. However, in the BB, the gradient of BR is very low (i.e., 0.10–0.06 m/km).

The BR drains a catchment area of 580000 km^2 with more than half of this area lying within China and Tibet; the remaining includes parts of Bhutan, India and Bangladesh. The total length of the river is 2906 km with its source being the Kangklung Kang glacier in Tibet at an altitude of 4877 m (Boruah et al., 2008).

Upon coming out of the hilly tracts, the BR flows in a W–E direction through the Higher Himalayas, overturns at Arunachal and flows along a roughly E–W direction up to Guwahati, India (Fig. 2). After entering Bangladesh at Chilmari in the Kurigram district (Fig. 2), it flows in a N–S direction through the central part of the Brahmaputra floodplain and forms the Jamuna, crossing the Tista Plain and is joined by Ganges at Aricha on its way to the BoB. The Tista River (TR), another major river of Bangladesh, originates from the central part of lesser Himalayan and joins BR at Kurigram (Fig. 2). The BR floodplain is an active foreland basin formed as a result of continent–continent collision of the Indian plate with the Eurasian plate (Singh, 2009).

The BR flows through a wide variety of climatic conditions, from cold and frigid to sub-humid, from north to south in the Himalaya. In the deltaic plain, the climatic condition is humid sub-tropical and is preferably divided into three seasons such as cold season (November to February), hot season (March to mid-June) and the monsoon season (mid-June to October, when it receives the maximum rainfall). The deltaic plain has been divided into several geomorphic units as a result of fluvial incision in response to neotectonic events and climatic influence during the late Quaternary (Fig. 3). These geomorphic features include depositional surfaces that are associated with almost all the rivers on the BR floodplain. Morphologically, Coleman (1969) divided the BJR and its surroundings into 11 distinct geomorphological units: i) Jamuna floodplain; ii) Old Tista floodplain (east side of Jamuna); iii) Bangali–Hurasagar floodplain; iv) New Tista floodplain (west side of Jamuna); v) Old Brahmaputra floodplain; vi) Ganges floodplain; vii) Atraigur floodplain; viii) Daleswari floodplain; ix) Meghna floodplain; x) Pleistocene terrace (Madhupur and Barind Tract); and xi) undifferentiated Quaternary deposits (Fig. 3).

The bed load of the BJR consists of fine sand and silt. These sediments are characterized by high water content and are loosely compacted. The characteristics of the sediments and the high amount of materials imposed on the channels by the flow system cause the rivers to turn continuously, adjusting their bed configurations to differing flow regimes. In this regard, sediments in the BJR are not only deposited in millions of tons but are also highly susceptible to erosion when flow conditions alter (Coleman, 1969).

We have studied the sediment samples from the large river BJR draining the Himalayan collision zone (Fig. 1). The collision between India and Asia has originated the uplift of the most prominent topographic feature Himalaya on the Earth. Hence, the Himalayan

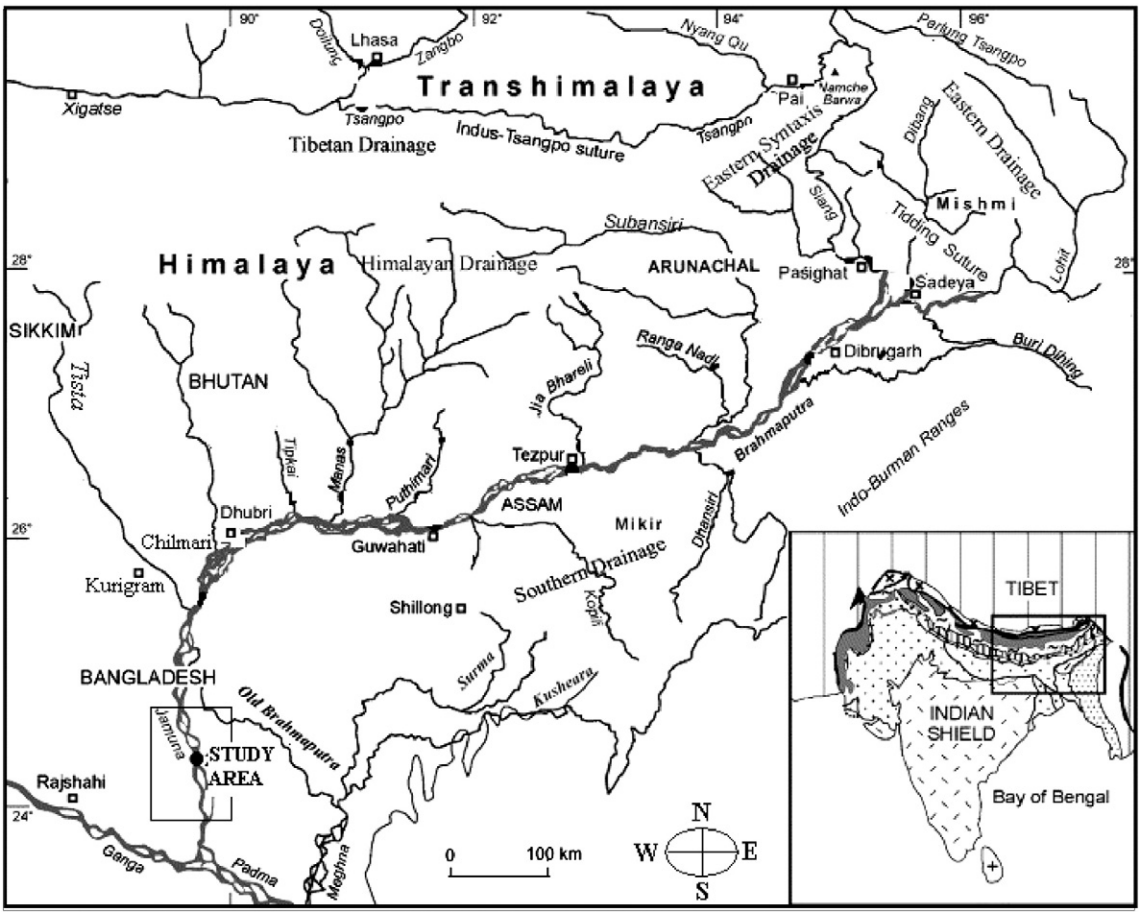

Fig. 2. Hydrologic framework of the study area (modified after Singh et al., 2006).

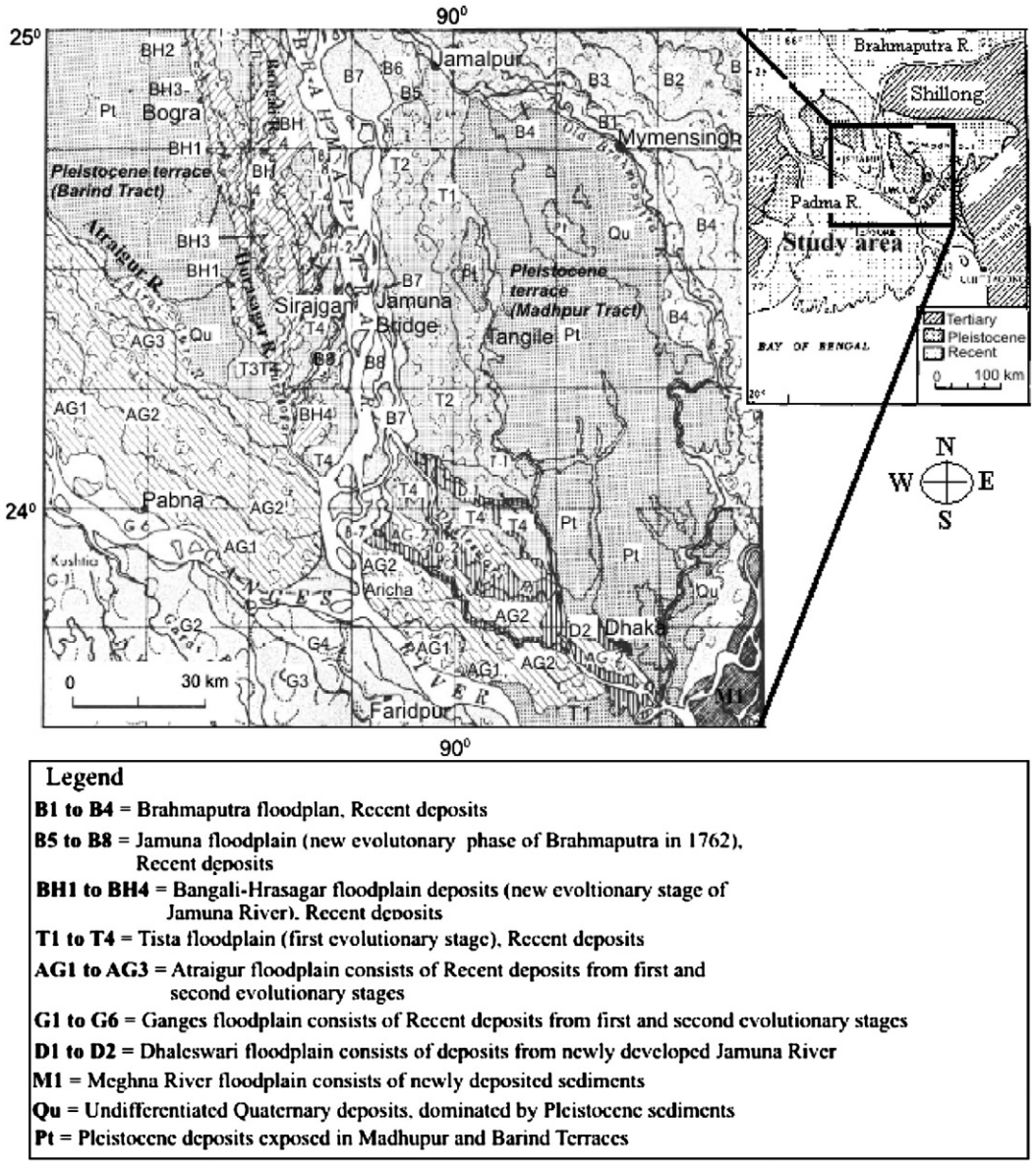

Fig. 3. Geology and geomorphic features in the study area (adopted from Coleman, 1969).

system is the leading source of terrigenous sediments nowadays, which are carried by the large Asian rivers (Indus, Ganges and Brahmaputra) originating here (~31%; ~4.2 109 t/yr) (Milliman and Meade, 1983). The sediments are finally deposited in submarine fans and provide a record of past tectonic and climatic history (Borges et al., 2008 and references therein). In high-relief areas with rapid transport and short duration of weathering, the study of fluvial sediments can reveal relationships between source rocks and eroded sediments. Because this source-rock signature is altered by the intensity and duration of weathering, which sequentially are influenced by climate and physiography (Grantham and Velbel, 1988). The sediments of the Indus and Ganges systems have been studied in detail for their petrography as well as isotopic compositions (Borges et al., 2008 and references therein), those of the BJR system have not benefited from such extensive focus till recently. Previous studies were conducted on geochemistry and some isotopic dating of Miocene sediments in the BB (e.g., France-Lanord et al., 1993; Galy and France-Lanord, 2001; Rahman and Suzuki, 2007). Study of the BJR sediments will enable to trace the development of the BB, the rise of which is the key mechanism for strengthening the southeast Asian monsoon system.

Geologically, the study area is surrounded by Pleistocene sediments that are exposed in the terraces of Madhupur and Barind at the eastern and western parts of the BJR system, respectively (Fig. 3). The relief of Madhupur Tract (MT) is quite high (average of ca. 30 m) and its gradient is gently inclined from north to south. The maximum altitudes of MT (ca. 70 m) are located along the western flank, where the boundary is incised by several en-echelon faults (Coleman, 1969). Even though the amount of throw on those faults is not known accurately, a bore log at Tangail, some 6 km west of the Pleistocene outcrop, intercepted the Pleistocene surface at a depth of ca. 70 m. Considering a minor regional slope, this would indicate a throw on the order of 50 m. From the western boundary of MT, the surface dips to the east and south and finally passes beneath the recent Brahmaputra floodplain deposit to the east (Coleman, 1969).

The structural activity within the MT is quite recent in origin, as evidenced by strong topographic dissections and high local relief, lack of deep valley filling, and the fresh nature of fault scarps. Ferguson (1963) argued that the MT had been uplifted and tilted in very recent times and referred to the earthquake of 1762, which was accompanied by rise and subsidence of large volume of landmass. This structural movement has contributed widely to the abandonment of the Old

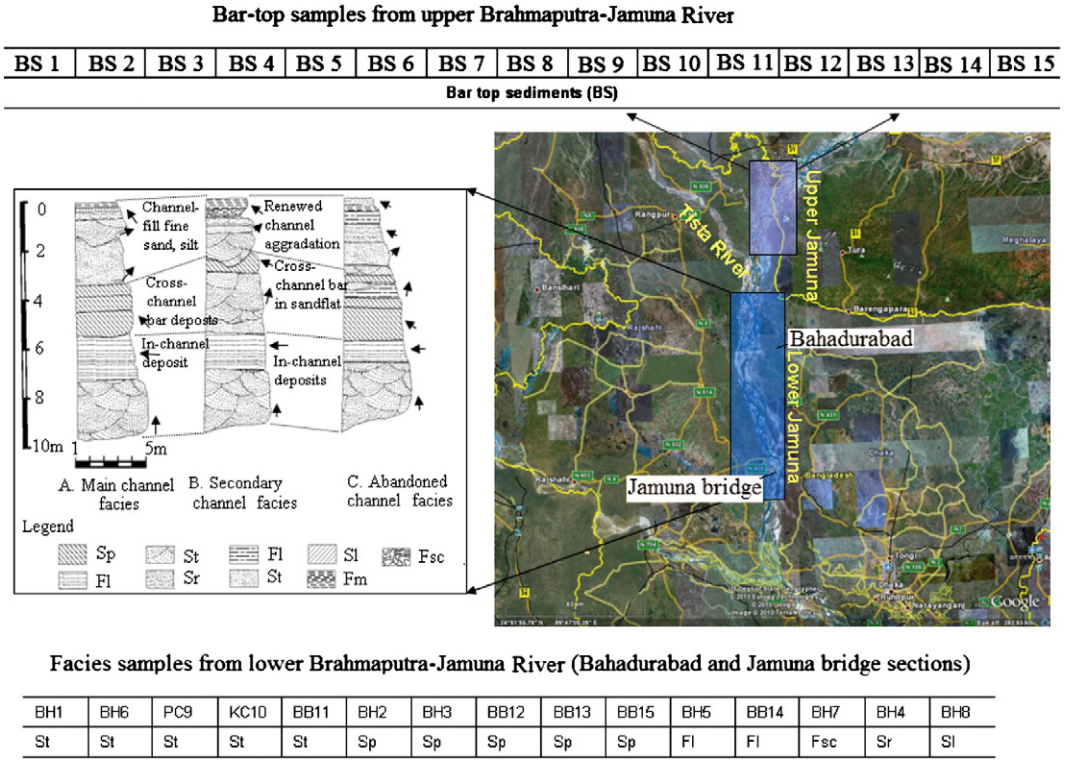

Fig. 4. Sampled sections of the Brahmaputra–Jamuna River. Sampling sites in the study area.

Brahmaputra to the east of the MT and preference to its present course at Jamuna-to the west of the MT.

Another major unit of Pleistocene sediment lies on the north-western part of the BJR and is referred to as the Barind Tract (BT) (Fig. 3) (Morgan and McIntire, 1959). The northeastern edge of this tract is terminated by a large fault that had a dominant influence on the course of the Karatoya–Bangali River. The elevation of this tract ranges from ca. 40 m in the north to ca. 10 m in the south. Local relief, however, is low, and there is practically no evidence of dissection. Structural movements in the BT have been active, but possibly consisted of broad block uplift or slight doming, as the terrace surface is essentially level. Several large abandoned-stream scars are evident on the surface, and are a sign of the fluvial origin of these sediments (Coleman, 1969).

Table 1
Mineralogy of the Brahmaputra–Jamuna River sediments.

Sample	Quartz	K-Feldspar	Plagioclase feldspar	Lithic	Mica	Heavy minerals
BS1	66.07	1.41	5.22	7.23	8.43	11.65
BS2	58.58	3.94	5.05	14.55	9.70	8.18
BS 3	64.79	0.80	6.54	14.48	2.21	11.17
BS 4	64.19	0.60	5.42	8.32	3.71	17.75
BS 5	63.37	3.57	9.90	11.83	6.33	5.00
BS 6	63.55	0.50	4.33	7.45	2.62	21.55
BS 7	58.45	3.00	4.60	13.02	7.61	13.31
BS 8	61.96	2.40	5.21	12.41	4.90	13.11
BS 9	65.70	1.71	5.92	10.43	6.42	9.83
BS 10	66.47	1.90	5.01	9.71	5.31	11.61
BS 11	64.35	1.11	6.75	11.08	3.22	13.49
BS 12	67.83	1.80	3.31	8.82	9.12	9.12
BS 13	56.60	4.20	6.30	15.20	7.60	10.10
BH1	69.55	1.50	4.76	3.71	5.67	14.81
BH2	59.30	2.24	7.12	5.69	17.16	8.50
BH3	73.49	4.16	7.15	7.01	1.20	7.00
BH4	65.15	4.20	7.25	10.00	5.20	8.20
BH5	68.09	3.50	6.62	5.90	3.50	12.40
BH6	64.06	2.97	7.21	8.39	9.25	8.14
BH7	67.92	2.90	5.45	9.13	6.60	8.00
BH8	68.10	3.22	6.40	7.86	6.17	8.28
PC9	72.20	4.10	4.65	7.63	5.13	6.31
KC10	67.76	2.25	6.20	7.38	7.30	9.20
BB11	70.51	2.11	5.12	6.28	7.49	8.50
BB12	65.91	3.25	6.14	6.65	5.95	12.12
BB13	63.17	1.85	7.20	7.16	5.80	14.82
BB14	68.60	2.40	6.25	5.15	7.60	10.00
BB15	70.36	3.10	5.20	6.31	5.54	9.50

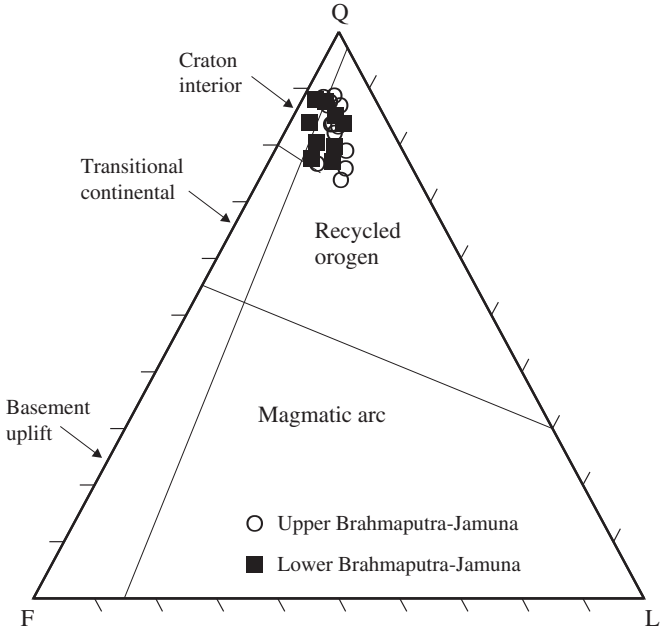

Fig. 5. Ternary plots of total quartz–feldspar–lithic fragments (QFL) data from the Brahmaputra–Jamuna River sediments and the classification of Dickinson (1985).

3. Methods

3.1. Sample collection and grain-size analysis

Thirty sediment samples (each weighing in the range of 2–3 kg) were collected from sand bars and various sedimentary facies units in the cut-bank exposures of upper and lower BJR when the river flowed through the base line (Fig. 4). Fifteen sand samples (prefixed with BS) were collected from bar-top at depths of 10–50 cm in freshly deposited sand bars of the upper BJR. Here, sediment samples were collected at certain depth (10–50 cm) due to avoid the anthropogenic interferences. It is mentioned that the reason behind this sampling strategy in upper BJR is that the sediments at this river section (Chilmari point) are mostly contributed from the BR. Another fifteen samples (prefixed with St, Sp, Fl, Fsc, Sr and Sl) were collected from different sedimentary facies units of the lower BJR, exposed in the erosional parts of sand bars and cut-bank exposures at depths of 20–30 cm. The sediments in this river section are not only contributed from the BR, also from the TR. Here, the logic behind such sampling strategy (bar-top and facies units) is two folds: (1) sediment samples in these facies units will help to understand the influence of grain-size variations on the sediment geochemistry, and (2) geochemical changes in sediments samples of the BR between before TR and after TR. These samples were named and coded individually following the scheme of Miall (1976) as large scale trough cross-stratified sandy facies (St), planar cross-stratified sandy facies (Sp), parallel laminated

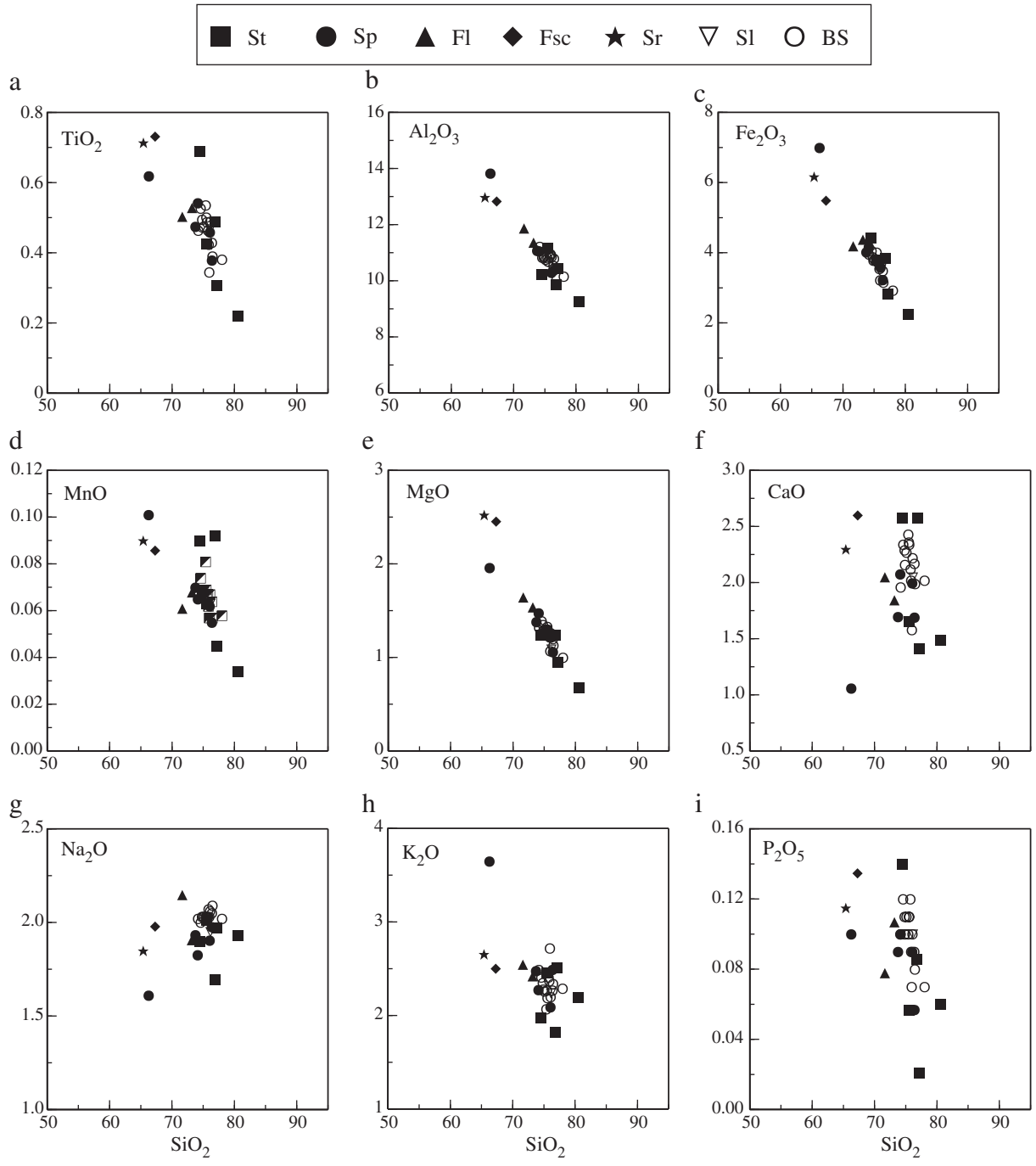

Fig. 6. Harker variation diagrams for major elements of the Brahmaputra–Jamuna River sediments.

fine sandy facies (Fl), ripple sand, silt and mud facies (Fsc), climbing ripple sand and silt facies (Sr), and low angle cross-stratified sandy facies (Sl). The facies sample locations were chosen on the availability of exposures in erosional bar sections and named after the local area manes. Samples collected from the upstream of Jamuna Bridge (Fig. 4) were prefixed with BH. Two samples (each prefixed with PC and KC), which collected from the downstream of the Jamuna Bridge, are located in Phular Char and Kaiser Char. Five samples (prefixed as BB) were collected from Bahadurabad area (midstream of the BJR).

All sediment samples were kept in pre-cleaned polyethylene bags and were transported to the laboratory. The samples were air-dried at room temperature. As the geochemistry of sand- to silt-sized sediments is useful in understanding the lithological (source region) control and sedimentary reworking during denudational processes, the samples were sieved to remove gravels and particles over 2 mm size. The grain-size analysis of sand-sized fractions was measured by sieving method. After sieving, 100 g of each sediment sample was ground to −200 mesh (<75 μm) size using agate mortar and pestle for geochemical study.

3.2. Mineralogical and geochemical study

Mineralogical study was conducted on 23 sand samples having size fractons of 63–500 μm (but dominant size class 63–250 μm) using a petrographic microscope. About 600 points per thin section were counted using the Gazzi–Dickinson point counting method as described by Ingersoll et al. (1984). For the presence of coarse mineral aggregates, such as quartz–feldspars aggregates, individual minerals were counted as single grains.

The geochemical analyses of 30 selected samples were performed at the Activation Laboratories Ltd. (Actlabs) (Code: 4Lithoresearch), Ontario, Canada. Oxides of the 10 traditionally listed major elements (Al, Si, Ti, Fe, Mn, Mg, Ca, Na, K and P) were analyzed by lithium metaborate/tetraborate fusion inductively coupled plasma (ICP) whereas trace elements and REEs were analyzed by inductively coupled plasma mass spectrometry (ICP-MS). Both analytical precision and accuracy for major elements are both better than 2%; whereas for trace elements and REE, analytical precision and accuracy are better than 2% and 5%, respectively. The detection limits for oxides (in %),

Table 2
Major element compositions (wt.%) and element ratios of the Brahmaputra–Jamuna River sediments.

Element	BS1	BS2	BS3	BS4	BS5	BS6	BS7	BS8	BS9	BS10	BS11	BS12	BS13	BS14	BS15
	Fine sand	Fine sand	Fine sand	Fine sand	Fine sand	Fine sand	Fine sand	Fine sand	Fine sand	Fine sand	Fine sand	Fine sand	Fine sand	Fine sand	Fine sand
SiO_2	75.83	77.98	76.35	75.93	74.78	75.07	75.72	76.05	74.55	75.46	75.53	74.15	74.84	75.37	76.44
Al_2O_3	10.96	10.16	10.54	10.94	10.84	10.76	10.85	10.86	10.83	10.70	10.69	11.22	10.88	10.81	10.79
Fe_2O_3(T)	3.55	2.93	3.49	3.22	3.88	3.80	3.71	3.69	4.06	3.76	3.74	3.96	3.78	4.01	3.16
MnO	0.06	0.06	0.06	0.06	0.07	0.07	0.07	0.07	0.07	0.07	0.07	0.07	0.07	0.08	0.06
MgO	1.22	1.00	1.20	1.07	1.35	1.30	1.26	1.26	1.39	1.33	1.30	1.32	1.29	1.30	1.13
CaO	2.02	2.02	2.17	1.58	2.29	2.27	2.12	2.22	2.34	2.36	2.34	1.96	2.16	2.43	1.99
Na_2O	2.07	2.02	2.05	2.03	2.03	2.03	2.03	2.06	2.00	2.03	2.03	2.02	2.03	2.03	2.09
K_2O	2.37	2.29	2.27	2.72	2.35	2.26	2.41	2.20	2.41	2.27	2.19	2.49	2.28	2.07	2.34
TiO_2	0.42	0.38	0.43	0.35	0.50	0.48	0.46	0.49	0.53	0.50	0.49	0.46	0.47	0.54	0.39
P_2O_5	0.09	0.07	0.09	0.07	0.11	0.11	0.12	0.10	0.12	0.11	0.11	0.10	0.10	0.10	0.08
LOI	1.19	0.93	1.12	1.40	1.21	1.18	1.16	1.04	1.22	1.07	1.08	1.42	1.28	0.94	0.99
Total	99.79	99.82	99.78	99.37	99.42	99.31	99.91	100.00	99.54	99.67	99.57	99.17	99.16	99.67	99.46
CIA	53.20	51.75	51.88	54.44	51.90	52.05	52.54	52.55	51.61	51.47	51.76	53.94	52.78	51.95	52.95
Na_2O/K_2O	0.87	0.88	0.90	0.75	0.86	0.90	0.84	0.94	0.83	0.89	0.93	0.81	0.89	0.98	0.89
K_2O/Na_2O	1.14	1.13	1.11	1.34	1.16	1.11	1.19	1.07	1.21	1.12	1.08	1.23	1.12	1.02	1.12
SiO_2/Al_2O_3	6.92	7.68	7.24	6.94	6.90	6.98	6.98	7.00	6.88	7.05	7.07	6.61	6.88	6.97	7.08
Al_2O_3/SiO_2	0.14	0.13	0.14	0.14	0.14	0.14	0.14	0.14	0.15	0.14	0.14	0.15	0.15	0.14	0.14
Fe_2O_3/K_2O	1.50	1.28	1.54	1.18	1.65	1.68	1.54	1.68	1.68	1.66	1.71	1.59	1.66	1.94	1.35
$Fe_2O_3 + MgO$	4.77	3.93	4.69	4.29	5.23	5.10	4.97	4.95	5.45	5.09	5.04	5.28	5.07	5.31	4.29
$CaO + Na_2O$	4.09	4.04	4.22	3.61	4.32	4.30	4.15	4.28	4.34	4.39	4.37	3.98	4.19	4.46	4.08

Element	St					Sp					Fl		Fsc	Sr	Sl
	BH1	BH6	PC9	KC10	BB11	BH2	BH3	BB12	BB13	BB15	BH5	BB14	BH7	BH4	BH8
	Fine sand	Fine sand	Fine sand	Fine sand	Fine sand	Silt, mud	Fine sand	Fine sand	Fine sand	Fine sand	Fine sand	Silt	Mud	Silt	Fine sand
SiO_2	77.09	74.41	80.48	76.77	75.44	66.23	76.4	74.09	73.7	76.01	71.59	73.13	67.23	65.37	76.12
Al_2O_3	10.46	10.25	9.26	9.86	11.18	13.83	10.4	11.06	11.1	10.3	11.88	11.37	12.85	12.98	10.24
Fe_2O_3(T)	2.84	4.42	2.27	3.86	3.81	7	3.23	4.17	4.02	3.59	4.2	4.39	5.5	6.17	3.66
MnO	0.05	0.09	0.03	0.09	0.06	0.1	0.06	0.07	0.07	0.06	0.06	0.07	0.09	0.09	0.06
MgO	0.95	1.24	0.68	1.25	1.29	1.96	1.06	1.48	1.38	1.22	1.65	1.54	2.46	2.53	1.09
CaO	1.42	2.58	1.49	2.58	1.66	1.06	1.69	2.08	1.7	2	2.05	1.85	2.61	2.3	2.05
Na_2O	1.97	1.9	1.93	1.7	2.01	1.61	1.98	1.83	1.93	1.9	2.15	1.91	1.98	1.85	1.95
K_2O	2.52	1.98	2.2	1.83	2.46	3.65	2.49	2.28	2.48	2.09	2.55	2.43	2.51	2.66	2.24
TiO_2	0.31	0.69	0.22	0.49	0.43	0.62	0.38	0.54	0.48	0.46	0.5	0.53	0.73	0.71	0.47
P_2O_5	0.02	0.14	0.06	0.09	0.06	0.1	0.06	0.1	0.09	0.09	0.08	0.11	0.14	0.12	0.1
LOI	1.19	0.87	0.74	0.73	1.49	3.41	1.06	1.4	1.67	1.1	1.88	1.65	3.11	3.9	1.01
Total	98.8	98.57	99.37	99.24	99.88	99.59	98.8	99.08	98.6	98.82	98.59	98.96	99.2	98.66	98.99
CIA	55.05	50.72	52.84	51.04	55.44	61.86	53.5	54.47	55.3	53.3	54.24	55.49	54.54	52.25	56.25
Na_2O/K_2O	0.78	0.96	0.88	0.93	0.82	0.44	0.79	0.8	0.78	0.91	0.84	0.79	0.79	0.87	0.7
K_2O/Na_2O	1.28	1.04	1.14	1.08	1.22	2.27	1.26	1.25	1.28	1.1	1.19	1.27	1.27	1.15	1.44
SiO_2/Al_2O_3	7.37	7.26	8.69	7.78	6.75	4.79	7.36	6.7	6.65	7.38	6.03	6.43	5.23	7.43	5.04
Al_2O_3/SiO_2	0.14	0.14	0.12	0.13	0.15	0.21	0.14	0.15	0.15	0.14	0.17	0.16	0.19	0.13	0.2
Fe_2O_3/K_2O	1.13	2.23	1.03	2.11	1.55	1.92	1.3	1.83	1.62	1.71	1.65	1.81	2.19	1.63	2.32
$Fe_2O_3 + MgO$	3.79	5.66	2.95	5.1	5.09	8.96	4.29	5.65	5.4	4.8	5.84	5.93	7.96	4.75	8.7
$CaO + Na_2O$	3.39	4.48	3.42	4.28	3.67	2.67	3.67	3.9	3.63	3.9	4.2	3.75	4.59	4	4.15

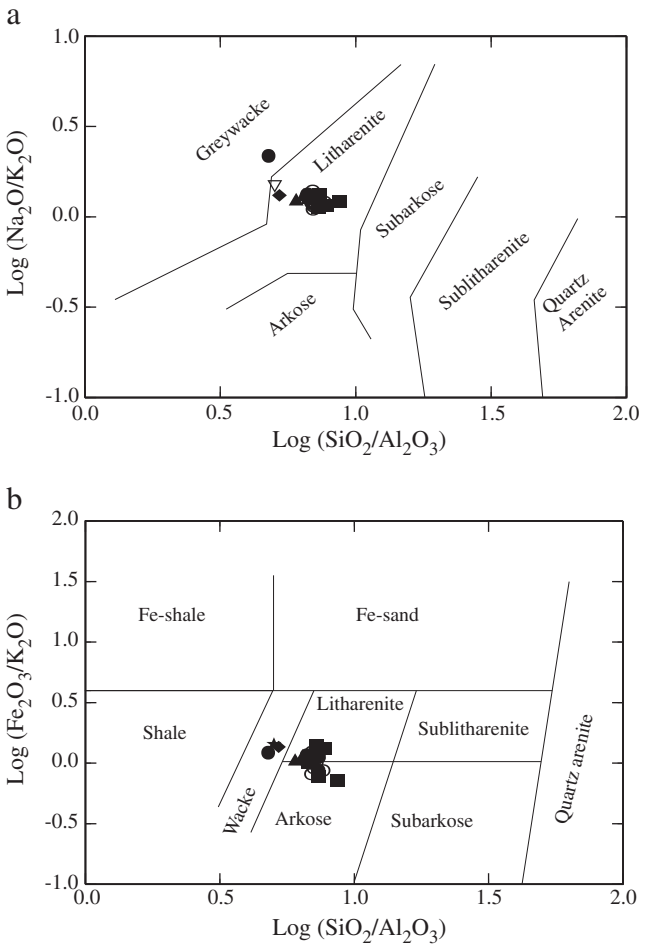

Fig. 7. Geochemical classifications of the Brahmaputra–Jamuna River sediments (a) after Pettijohn et al., 1995 and (b) Herron, 1986. Legends of plot symbols are as shown in Fig. 6.

trace elements and REEs (in ppm) are: 0.01(SiO_2, Al_2O_3, Fe_2O_3, MgO, CaO, Na_2O, K2O, P_2O_5), 0.001(MnO, TiO_2), 20 (Cr, Ni), 10 (Cu), 30 (Zn), 5 (V, As, Pb), 2 (Sr, Mo), 1 (Co, Ga, Rb, Zr, Sn), 0.5 (Ge, Y, Ag,W), 0.2 (Nb, Sb), 0.1 (In, Cs, Yb, Hf, Bi), 3 (Ba), 0.05 (La, Ce, Nd, Tl, Th), 0.01 (Pr, Yb, Sm, Gd, Tb, Dy, Ho, Er, Ta, U), 0.002 (Lu) and 0.005 (Eu, Tm).

3.3. Methods of geochemical data interpretation

Recently, the total quartz–feldspars–lithic fragments (QFL) diagrams had gained more importance in areas with clear tectonic distinction. For example, QFL diagrams indicate extremely quartzose recycled orogen provenance of Brazilian river sands and Transitional Arc provenance for Argentine and South American Pacific coastal sands (Potter, 1994).

Moreover, QFL diagrams indicate a recycled orogen provenance of the Lena River sands, and samples of platform and shield sediments, whereas QFL diagrams indicate an Arc provenance of samples of collision zone sediments (Potter et al., 2001). Besides QFL diagrams, the bivariate and discriminant function diagrams using major oxides have been proposed (Bhatia, 1983; Roser and Korsch, 1986) to infer tectonic provenance.

Numerous classification schemes have been proposed to discriminate sediments according to origin and tectonic setting (e.g., Bhatia, 1983; Bhatia and Crook, 1986; Maynard et al., 1982; Roser and Korsch, 1986, 1988). Tectonic provenance of sands and sandstones is frequently inferred from discrimination diagrams using petrographic data and major oxide data (Borges et al., 2008). Although such diagrams have limited utility in providing coherent tectonic setting information, they may illustrate local lithology. In addition discrimination diagrams are convenient for viewing stratigraphic variations among sediments. The ratio of discriminant functions of Roser and Korsch (1988) utilizes ratios of TiO_2, Fe_2O_3T, MgO, CaO, Na_2O and K_2O to Al_2O_3 and classifies sandstones–mudstones groups into four sedimentary provenance types such as mafic and lesser intermediate igneous provenance; intermediate igneous provenance; felsic igneous provenance and recycled-mature polycyclic quartzose detritus.

Bivariate plots have also proved useful in discriminating terrigenous sediments from upper continental crust (UCC) in terms of SiO_2, Na_2O and K_2O contents. Roser and Korsch (1986) proposed a bivariate tectonic discrimination diagram using K_2O/Na_2O versus SiO_2 to determine the tectonic setting of terrigenous sedimentary rocks. Concentrations of SiO_2 and K_2O/Na_2O increase from volcanic-arc to active continental margin (ACM) to passive margin (PM) settings. However, Armstrong-Altrin and Verma (2005) demonstrated, in their study of Neogene sediments from known tectonic settings, that the major oxide bivariate and discriminant function diagrams do not perform reliably. Nevertheless, Armstrong-Altrin and Verma (2005) proposed that the K_2O/Na_2O vs. SiO_2 tectonic classification diagram (Roser and Korsch, 1986) yielded quite better results than the others and had good success rate of classification.

The chemistry of sediments is a result of net influence of provenance, weathering and fluvial processes involved in sorting (McLennan et al., 1993; Rollinson, 1993). The bulk change in the chemistry of sediments can be associated with weathering according to the chemical index of alteration (CIA), which is used to quantify weathering intensity due to progressive alteration of plagioclase and potassium feldspars to clay minerals. The CIA is computed using molar proportions of oxides following the equation $CIA = [Al_2O_3/(Al_2O_3 + CaO^* + Na_2O + K_2O)] \times 100$, where CaO^* represents the amount of CaO integrated in the silicate phases. According to Nesbitt and Young (1984), high values of CIA (i.e., 76–100) represent intensive chemical weathering in the source areas whereas low values of CIA (i.e., 50 or less) signify unweathered source areas.

The high-field-strength elements (HFSE) such as Zr, Nb, Hf, Y, and Th are thought to reflect provenance compositions because of their general immobile behavior (Taylor and McLennan, 1985). These elements are preferentially partitioned into melts during crystallization (Feng and Kerrich, 1990), and consequently are derived mainly from felsic sources but with some contribution from mafic source. Besides, HFSEs, REEs and Sc provide evidence of source compositions due to their comparatively low mobility during sedimentation and their low residence times in sea water (Bhatia and Crook, 1986). Concentrations of REEs and Th abundances are generally higher in felsic igneous source rocks compared to mafic igneous source rocks and in their weathered products, whereas Co, Sc, and Cr generally have higher concentrations in mafic than in felsic igneous source rocks and/or in their weathered products. Mafic and felsic source rocks also differ significantly in element ratios such as Eu/Eu*, $(La/Lu)_N$, La/Sc, Th/Sc, La/Co, Th/Co and Cr/Th, and therefore provide useful information about the provenance of sedimentary rocks (e.g., Cullers, 1994, 2000; Cullers et al., 1988; Cullers and Podkovyrov, 2000). The use of element ratios has the advantage that they are independent of dilution effects, such as that produced by quartz in sediments. Element ratios can be fractionated during weathering and transport (Rollinson, 1993), and during sorting and heavy mineral concentration (Roser et al., 2000). Correlations were done to identify the association and level of significance of elements in the correlation matrix.

4. Results and analysis

4.1. Grain-size variations

The grain-size parameters of fluvial sediments exposed in the different sedimentary facies units of the lower BJR were analyzed to aid in determining the interpretation of the variations in the geochemistry of fluvial sediments. The bar-top sediments in the upper part of the BJR

have a mean size (Mz) of 2.15φ (fine sand), which varies within a narrow range of 2.01–2.32φ. However, in most of the studied samples from the different sedimentary facies units, the Mz varies from 2.01φ (fine sand) to 4.25φ (mud), though only one sample was medium sized-sand (1.73φ). Due to variation in bar-top sediment, the mean grain size of bar-top samples was used for geochemical analysis. Standard deviation (σ) ranges from 0.31φ (very well sorted) to 0.76φ (moderately sorted). Skewness (SK1) also varies from −0.44φ (strongly coarse skewed) to 0.28φ (fine skewed). Large scale trough cross-stratified sandy facies (St) and planer cross-stratified sandy facies (Sp) consist mostly of fine sands whereas parallel laminated sandy facies (Fl), rippled facies (Sr) contain mostly very fine sands, silts and muds.

4.2. Petrography

The minerals identified in the bar-top and channel facies unit sediments comprise quartz, plagioclase feldspars, K-feldspars and mica as dominant phases. In addition, some feldspathic and quartz arenites are also recognized. Quartz is the main constituent mineral, comprising about 65.6% of the sediment volume and occurring as monocrystalline (most abundant) and polycrystalline grains. Feldspar constitutes about 8.5% of the total volume of minerals, with plagioclase dominating over K-feldspar (Table 1). Heavy mineral assemblage (average composition of 11%; Table 1) is characterized by predominance of amphibole, epidote, garnet and apatite. Lithic fragments, comprising mainly sedimentary and low-grade metamorphic lithics, and minor volcanic detritus, constitute about 9% of the bulk sediment composition. The bulk of the BJR sediments contain abundant quartz and little of both feldspars and lithic fragments which indicate that they, based on their mineral compositions, were most likely derived from a quartzose recycled orogen province (Fig. 5) (cf. Dickinson, 1985).

4.3. Geochemistry

4.3.1. Major elements

In general, samples of sediments from the different sedimentary facies units (fine sand to muds) and bar-top (fine sands) of the BJR have moderate (ca. 65%) to high (ca. 80%) SiO_2 contents with a mean ca. 75% SiO_2 probably because of their high quartz contents (Table 1). In general, the sediment samples of facies units have higher Al_2O_3, Fe_2O_3, MgO, MnO, TiO_2 and K_2O compared to the bar-top sediments in the studied sections of the fluvial system of BJ. The negative linear

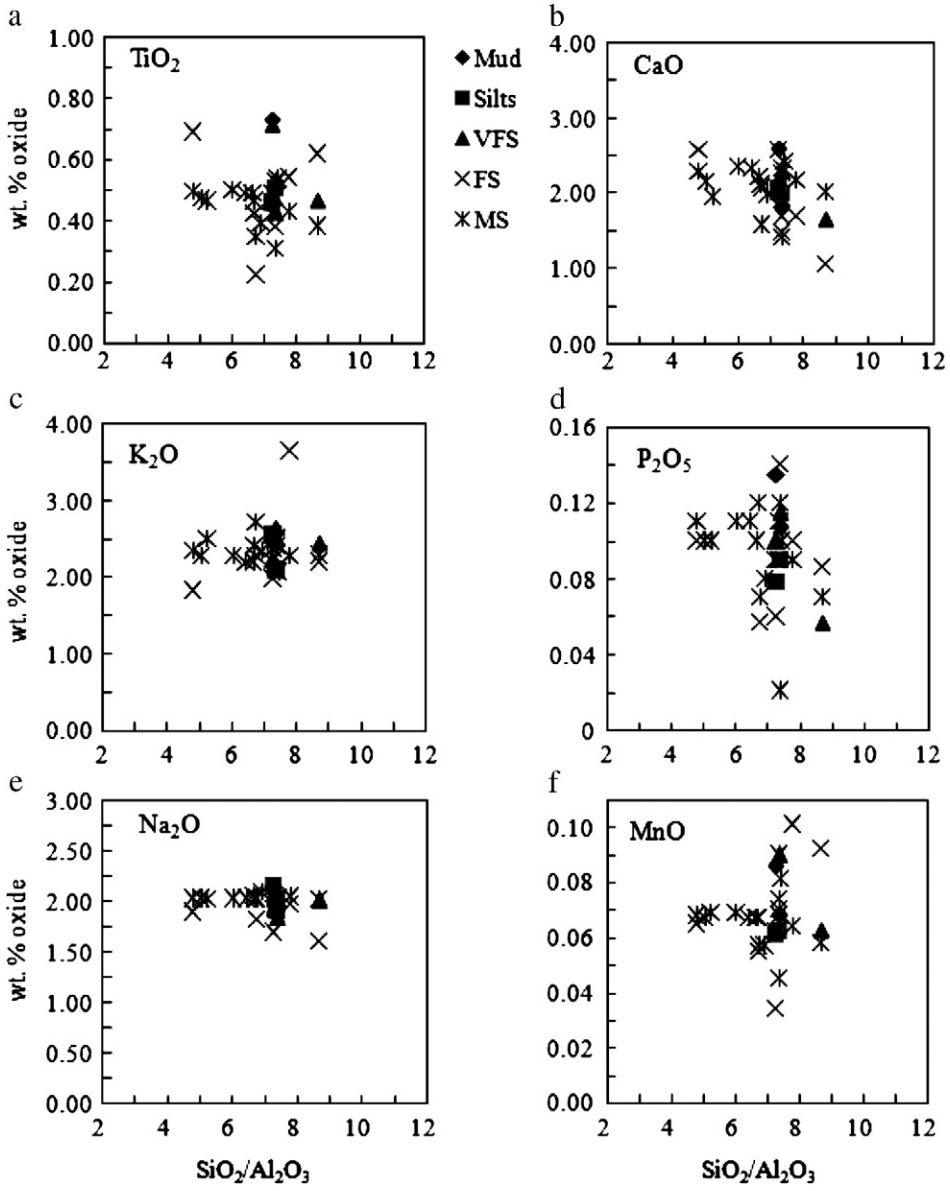

Fig. 8. Oxide (wt.%)–SiO_2/Al_2O_3 variation diagrams, by grain-size class. BFS = bar-top fine sand; FFS = facies fine sand; VFS = very fine sand.

Table 3
Trace and rare earth element compositions (ppm) and element ratios of the Brahmaputra–Jamuna River sediments.

Element	BS1	BS2	BS3	BS4	BS5	BS6	BS7	BS8	BS9	BS10	BS11	BS12	BS13	BS14	BS15
	Fine sand	Fine sand	Fine sand	Fine sand	Fine sand	Fine sand	Fine sand	Fine sand	Fine sand	Fine sand	Fine sand	Fine sand	Fine sand	Fine sand	Fine sand
Sc	8.00	8.00	9.00	7.00	10.00	10.00	9.00	9.00	10.00	10.00	10.00	9.00	9.00	10.00	8.00
Be	2.00	2.00	2.00	2.00	2.00	2.00	2.00	2.00	2.00	2.00	2.00	2.00	2.00	2.00	2.00
V	53.00	47.00	55.00	45.00	61.00	59.00	58.00	57.00	65.00	62.00	59.00	58.00	58.00	61.00	50.00
Cr	40.00	30.00	40.00	40.00	50.00	50.00	50.00	50.00	50.00	50.00	50.00	50.00	50.00	50.00	30.00
Co	9.00	5.00	8.00	8.00	9.00	9.00	9.00	8.00	9.00	9.00	8.00	10.00	8.00	6.00	6.00
Ni	<20	<20	<20	<20	<20	<20	<20	<20	<20	<20	<20	<20	<20	<20	<20
Cu	40.00	<10	<10	<10	<10	<10	<10	<10	<10	<10	20.00	30.00	<10	20.00	10.00
Zn	40.00	<30	30.00	40.00	40.00	40.00	40.00	40.00	40.00	40.00	40.00	40.00	<30	<30	30.00
Ga	13.00	11.00	12.00	13.00	13.00	13.00	13.00	12.00	14.00	14.00	13.00	14.00	12.00	10.00	11.00
Ge	1.60	1.20	1.40	1.50	1.60	1.40	1.50	1.40	1.30	1.60	1.50	1.20	1.30	1.50	1.30
Rb	105.00	80.00	87.00	118.00	95.00	90.00	100.00	90.00	100.00	94.00	89.00	113.00	90.00	79.00	90.00
Sr	178.00	177.00	181.00	167.00	180.00	182.00	178.00	180.00	182.00	182.00	184.00	175.00	178.00	186.00	181.00
Y	20.70	19.50	21.30	17.00	25.30	24.20	22.90	28.10	29.20	29.50	26.80	21.90	21.40	28.60	19.90
Zr	153.00	153.00	164.00	103.00	221.00	205.00	176.00	192.00	230.00	263.00	240.00	197.00	194.00	284.00	148.00
Nb	7.40	6.00	7.10	6.20	7.70	7.30	7.30	8.60	9.40	8.30	7.60	7.80	7.00	7.60	6.20
Cs	5.40	3.00	4.00	6.10	4.80	4.40	5.10	4.00	5.30	4.40	4.30	6.50	4.60	3.60	4.40
Ba	399.00	374.00	373.00	427.00	372.00	375.00	389.00	381.00	370.00	368.00	366.00	413.00	383.00	368.00	393.00
La	27.20	26.80	29.10	19.30	31.60	30.90	29.40	31.90	37.60	39.80	37.60	29.30	29.20	37.20	24.90
Ce	52.30	51.20	56.80	37.80	61.40	60.00	57.60	61.20	72.30	76.40	73.30	56.70	57.90	72.20	48.20
Pr	5.88	5.69	6.40	4.23	6.99	6.85	6.54	6.96	8.22	8.46	8.23	6.42	6.49	8.08	5.45
Nd	21.60	20.80	23.60	16.00	26.00	25.30	24.40	25.30	30.60	31.00	30.70	23.40	24.20	29.40	20.00
Sm	3.99	3.67	4.47	3.04	4.83	4.72	4.46	4.81	5.56	5.61	5.58	4.33	4.63	5.33	3.51
Eu	0.89	0.84	0.94	0.82	1.06	0.99	0.95	1.06	1.10	1.10	1.12	0.95	0.94	1.09	0.80
Gd	3.76	3.46	4.10	3.04	4.59	4.42	4.26	4.72	5.08	5.17	5.13	4.14	4.25	4.80	3.50
Tb	0.57	0.54	0.59	0.47	0.69	0.68	0.65	0.74	0.80	0.78	0.74	0.62	0.64	0.80	0.56
Dy	3.19	2.97	3.49	2.80	3.98	3.86	3.72	4.28	4.48	4.57	4.30	3.58	3.69	4.44	3.09
Ho	0.62	0.59	0.68	0.56	0.80	0.76	0.72	0.86	0.89	0.90	0.84	0.70	0.70	0.89	0.60
Er	1.79	1.75	2.01	1.63	2.29	2.26	2.07	2.56	2.52	2.60	2.47	2.08	2.09	2.64	1.81
Tm	0.27	0.28	0.31	0.24	0.36	0.35	0.31	0.39	0.38	0.39	0.37	0.32	0.32	0.43	0.28
Yb	1.69	1.83	1.97	1.51	2.31	2.18	1.97	2.41	2.36	2.48	2.41	2.02	2.01	2.74	1.72
Lu	0.24	0.26	0.27	0.21	0.32	0.29	0.29	0.33	0.35	0.37	0.36	0.29	0.28	0.38	0.25
Hf	3.80	3.80	4.00	2.70	5.50	4.90	4.50	4.70	6.00	6.60	6.40	5.20	4.70	6.90	3.90
Ta	0.69	0.71	0.79	0.67	0.92	0.74	0.73	1.06	1.08	0.95	0.78	0.81	0.75	0.89	0.73
W	2.00	1.50	1.40	1.80	1.80	2.30	1.60	1.60	1.50	1.50	1.60	1.70	1.40	1.30	1.40
Tl	0.45	0.31	0.43	0.60	0.46	0.35	0.51	0.47	0.44	0.40	0.47	0.50	0.46	0.36	0.49
Pb	18.00	14.00	19.00	23.00	17.00	14.00	20.00	19.00	17.00	17.00	19.00	17.00	16.00	15.00	19.00
Bi	0.30	0.20	0.30	0.40	0.30	0.30	0.30	0.30	0.30	0.30	0.40	0.30	0.30	0.30	0.30
Th	11.40	10.60	12.30	7.44	13.70	12.80	12.70	14.50	17.50	17.40	15.20	12.60	12.90	15.60	10.80
U	2.08	1.79	2.08	1.40	2.32	2.25	2.13	2.28	3.15	2.72	2.49	2.22	2.00	2.57	1.98
Rb/Sr	0.59	0.45	0.48	0.71	0.53	0.49	0.56	0.50	0.55	0.52	0.48	0.65	0.51	0.42	0.50
Th/Sc	1.43	1.33	1.37	1.06	1.37	1.28	1.41	1.61	1.75	1.74	1.52	1.40	1.43	1.56	1.35
Zr/Sc	19.13	19.13	18.22	14.71	22.10	20.50	19.56	21.33	23.00	26.30	24.00	21.89	21.56	28.40	18.50
Cr/Th	3.51	2.83	3.25	5.38	3.65	3.91	3.94	3.45	2.86	2.87	3.29	3.97	3.88	3.21	2.78
Th/Co	1.27	2.12	1.54	0.93	1.52	1.42	1.41	1.81	1.94	1.93	1.90	1.26	1.61	2.60	1.80
La/Co	3.02	5.36	3.64	2.41	3.51	3.43	3.27	3.99	4.18	4.42	4.70	2.93	3.65	6.20	4.15
La/Sc	3.40	3.35	3.23	2.76	3.16	3.09	3.27	3.54	3.76	3.98	3.76	3.26	3.24	3.72	3.11
La/SmN	4.29	4.60	4.10	4.00	4.12	4.12	4.15	4.17	4.26	4.47	4.24	4.26	3.97	4.39	4.47
La/YbN	10.88	9.90	9.98	8.64	9.24	9.58	10.08	8.94	10.77	10.84	10.54	9.80	9.82	9.17	9.78
Eu/Eu*	0.70	0.72	0.67	0.83	0.69	0.66	0.66	0.68	0.63	0.62	0.64	0.68	0.65	0.66	0.69
Ce/Ce*	0.97	0.97	0.98	0.98	0.97	0.97	0.97	0.96	0.96	0.98	0.98	0.97	0.99	0.98	0.97
Gd/YbN	1.80	1.53	1.69	1.63	1.61	1.64	1.75	1.59	1.74	1.69	1.73	1.66	1.71	1.42	1.65
La/LuN	11.91	10.87	11.15	9.59	10.16	10.91	10.63	10.19	11.06	11.29	10.84	10.64	10.94	10.14	10.55
	St					Sp					Fl		Fsc	Sr	Sl
	BH1	BH6	PC9	KC10	BB11	BH2	BH3	BB12	BB13	BB15	BH5	BB14	BH7	BH4	BH8
	Fine sand	Fine sand	Fine sand	Fine sand	Fine sand	Silt, mud	Fine sand	Fine sand	Fine sand	Fine sand	Fine sand	Silt	Mud	Silt	Fine sand
Sc	6.27	11.00	5.00	10.69	7.96	11.00	7.48	9.69	8.66	8.92	8.97	9.58	12.39	12.03	8.00
Be	2.23	2.00	2.00	1.90	2.31	3.00	2.52	2.43	3.39	2.14	2.35	2.55	2.27	2.40	2.00
V	40.39	78.00	33.00	65.14	55.95	86.00	49.61	67.78	57.97	57.32	64.94	62.92	93.85	94.48	57.00
Cr	30.00	80.00	20.00	50.00	40.00	60.00	40.00	50.00	50.00	50.00	50.00	50.00	80.00	80.00	40.00
Co	5.00	8.00	4.00	7.00	9.00	21.00	7.00	9.00	9.00	7.00	10.00	10.00	14.00	16.00	7.00
Ni	<20	20.00	<20	<20	30.00	50.00	<20	20.00	20.00	<20	20.00	20.00	40.00	40.00	20.00
Cu	20.00	<10	<10	20.00	<10	<10	<10	10.00	10.00	<10	20.00	20.00	30.00	50.00	<10
Zn	<30	40.00	<30	<30	<30	90.00	<30	<30	<30	<30	<30	30.00	50.00	40.00	30.00
Ga	11.00	13.00	10.00	12.00	13.00	19.00	12.00	13.00	13.00	12.00	13.00	14.00	16.00	16.00	12.00
Ge	1.40	1.90	1.50	1.80	1.70	2.00	1.60	1.90	1.60	1.70	1.60	1.60	1.90	1.80	1.80
Rb	109.00	78.00	83.00	68.00	113.00	229.00	107.00	104.00	138.00	95.00	119.00	121.00	114.00	132.00	91.00
Sr	161.60	183.00	164.00	176.50	161.70	134.00	165.60	158.40	152.10	163.00	180.90	145.60	191.60	177.90	175.00
Y	12.90	37.30	12.20	33.00	17.00	15.00	18.80	26.20	31.40	24.40	20.50	23.90	30.50	25.30	23.50
Zr	138.00	509.00	107.00	134.00	149.00	158.00	200.00	296.00	441.00	336.00	241.00	280.00	292.00	249.00	270.00

Table 3 (*continued*)

	St					Sp					Fl		Fsc	Sr	Sl
	BH1	BH6	PC9	KC10	BB11	BH2	BH3	BB12	BB13	BB15	BH5	BB14	BH7	BH4	BH8
	Fine sand	Fine sand	Fine sand	Fine sand	Fine sand	Silt, mud	Fine sand	Fine sand	Fine sand	Fine sand	Fine sand	Silt	Mud	Silt	Fine sand
Nb	32.50	14.20	5.70	11.60	9.90	15.90	12.70	12.60	38.80	12.30	24.30	15.10	16.00	15.80	9.30
Cs	4.40	3.10	2.70	2.10	5.50	19.30	4.40	4.90	5.90	3.80	5.00	5.90	5.70	6.70	3.90
Ba	432.20	348.00	380.00	318.50	433.00	612.00	423.90	400.40	416.50	366.70	449.10	408.60	447.50	469.80	386.00
La	19.40	67.00	19.40	66.90	26.60	21.70	30.30	42.40	35.90	39.80	27.10	38.80	43.20	34.40	42.20
Ce	35.90	126.00	35.40	121.00	49.20	40.30	55.10	78.90	67.10	73.30	51.10	71.70	81.40	64.50	77.20
Pr	4.02	13.80	4.04	13.10	5.49	4.59	6.02	8.73	7.37	8.10	5.79	7.98	9.38	7.36	8.77
Nd	14.50	49.70	14.40	45.50	19.90	17.00	22.10	31.70	26.40	29.40	21.30	29.10	34.10	27.30	30.90
Sm	2.87	9.33	2.76	7.95	3.80	3.38	4.22	6.13	5.37	5.72	4.29	5.52	6.75	5.53	5.89
Eu	0.65	1.36	0.67	1.22	0.80	0.77	0.81	1.03	0.88	0.98	0.88	0.99	1.45	1.05	1.02
Gd	2.39	7.23	2.38	6.26	3.31	2.99	3.59	5.14	4.90	4.78	3.65	4.66	5.94	4.73	4.76
Tb	0.36	1.13	0.39	0.98	0.49	0.48	0.56	0.80	0.84	0.73	0.58	0.74	1.13	0.75	0.78
Dy	2.27	6.75	2.26	5.96	3.05	2.75	3.41	4.66	5.37	4.33	3.59	4.29	5.51	4.40	4.45
Ho	0.43	1.34	0.47	1.19	0.58	0.56	0.66	0.90	1.13	0.85	0.72	0.82	1.07	0.88	0.89
Er	1.30	3.85	1.27	3.47	1.73	1.58	1.96	2.58	3.60	2.46	2.17	2.38	3.09	2.56	2.54
Tm	0.21	0.57	0.20	0.58	0.30	0.23	0.34	0.43	0.65	0.43	0.38	0.40	0.46	0.43	0.38
Yb	1.34	3.95	1.30	3.40	1.70	1.56	2.03	2.62	4.04	2.51	2.25	2.34	3.02	2.46	2.52
Lu	0.16	0.59	0.17	0.46	0.22	0.22	0.26	0.35	0.57	0.34	0.31	0.33	0.60	0.35	0.34
Hf	3.10	11.80	2.40	2.90	3.30	3.60	4.60	6.30	10.00	7.20	5.40	6.00	6.60	5.50	6.10
Ta	0.79	1.09	0.38	0.84	0.71	1.13	0.90	0.90	1.96	0.88	1.26	0.96	1.13	0.94	0.73
W	<0.5	<0.5	1.00	<0.5	<0.5	6.30	<0.5	<0.5	<0.5	<0.5	<0.5	<0.5	<0.5	<0.5	0.80
Tl	0.11	0.28	0.29	0.12	0.17	0.93	0.15	0.24	0.13	0.14	0.16	0.24	0.38	0.21	0.33
Pb	7.00	18.00	19.00	9.00	11.00	30.00	10.00	11.00	7.00	10.00	8.00	10.00	14.00	10.00	19.00
Bi	<0.1	<0.1	<0.1	<0.1	<0.1	0.30	<0.1	<0.1	<0.1	<0.1	<0.1	<0.1	2.20	<0.1	<0.1
Th	7.34	25.60	7.36	20.50	9.71	7.90	11.30	15.70	14.90	15.40	10.10	13.80	16.70	12.60	16.80
U	1.52	4.19	1.42	2.41	2.09	2.49	2.12	3.08	2.87	2.89	2.09	2.78	3.78	2.96	3.02
Rb/Sr	0.67	0.43	0.51	0.39	0.70	1.71	0.65	0.66	0.91	0.58	0.66	0.83	0.59	0.74	0.52
Th/Sc	1.17	2.33	1.47	1.92	1.22	0.72	1.51	1.62	1.72	1.73	1.13	1.44	1.35	1.05	2.10
Zr/Sc	22.02	46.27	21.40	12.54	18.71	14.36	26.76	30.54	50.94	37.69	26.86	29.24	23.57	20.70	33.75
Cr/Th	4.09	3.13	2.72	2.44	4.12	7.59	3.54	3.18	3.36	3.25	4.95	3.62	4.79	6.35	2.38
Th/Co	1.47	3.20	1.84	2.93	1.08	0.38	1.61	1.74	1.66	2.20	1.01	1.38	1.19	0.79	2.40
La/Co	3.88	8.38	4.85	9.56	2.96	1.03	4.33	4.71	3.99	5.69	2.71	3.88	3.09	2.15	6.03
La/Sc	3.10	6.09	3.88	6.26	3.34	1.97	4.05	4.37	4.15	4.46	3.02	4.05	3.49	2.86	5.28
La/SmN	4.25	4.52	4.42	5.30	4.41	4.04	4.52	4.35	4.21	4.38	3.98	4.42	4.03	3.92	4.51
La/YbN	9.78	11.46	10.08	13.30	10.57	9.40	10.09	10.94	6.00	10.72	8.14	11.20	9.67	9.45	11.32
Eu/Eu*	0.76	0.51	0.80	0.53	0.69	0.74	0.63	0.56	0.52	0.57	0.68	0.60	0.70	0.63	0.59
Ce/Ce*	0.95	0.97	0.94	0.96	0.95	0.95	0.96	0.96	0.97	0.96	0.96	0.95	0.95	0.95	0.94
Gd/YbN	1.45	1.48	1.48	1.49	1.58	1.55	1.43	1.59	0.98	1.54	1.31	1.61	1.59	1.56	1.53
La/LuN	12.43	11.89	11.71	15.13	12.61	10.29	12.05	12.76	6.57	12.12	9.08	12.39	7.46	10.26	12.74

relationships of SiO_2 with TiO_2, Al_2O_3, Fe_2O_3, MnO and MgO in the BJR sediments (Fig. 6) is due to most of the silica being sequestered in quartz (Rahman and Suzuki, 2007). The bar-top sediment samples (fine sands) show smaller variations in elemental concentration among the sample size. Major element compositions compared to the facies sediment samples (fine sand, very fine sand, silts and muds) (Table 2), on the other hand, show a considerable variation, which appears to be controlled by mean grain size of the sediments. For example, the SiO_2 concentrations in the fine sand (bar-top) samples have an average of 75.6% and a standard deviation of 0.93% whereas those in the facies samples (fine sands to muds) have an average of 73.6% and a standard deviation of 4.31%. This indicates that the coefficient of variation (CV) of SiO_2 in the facies samples (fine sands, silts and muds) is about five times higher than CV of SiO_2 in the bar-top samples. Similar observations are made for the other major oxides (TiO_2, Al_2O_3, Fe_2O_3, MnO, MgO, CaO, Na_2O, K_2O, and P_2O_5), where the CV values of their concentrations in the facies samples (fine sands, silts and muds) are 2–6 times higher than the CVs those in the bar-top samples (fine sands). Thus, it appears that variations in major element concentrations in the BJR fluvial sediments are influenced by grain-size variations and by distance from upstream to downstream section of the BJR in the study area.

Fluvial sediments are composite weathering products of lithologies in the catchment area of the river. Because the sediment samples of BJR are mostly sand, we normalized the major element compositions of the studied samples to that of an average sandstone as a reference for assessing elemental mobility during weathering and transport. Thus, compared to the mean of major element compositions of a sandstone reported by Turekian and Wedepohl (1961), the analyzed samples are depleted in CaO (2%), Al_2O_3 (11%), MgO (1.35%), Na_2O (1.97%), K_2O (2.38%), P_2O_5 (0.09%) but enriched in TiO_2 (0.5%), Fe_2O_3 (4%), MnO (0.068%), and Na_2O (2%). The minor depletions in K_2O and MgO are likely due to the dilution effect of silica, whereas depletions in Al_2O_3, CaO, Na_2O and K_2O are likely due to fluvial processes leading to preferential removal of fine-grained mica group of minerals but not feldspars in the suspended stream load (Singh, 2009).

According to the chemical compositional diagram of Pettijohn et al. (1995) and the compositional maturity diagram of Herron (1986), the BJR sediment samples are dominantly litharenites (Fig. 7). Textural maturity of sandstones can be evaluated by examining the SiO_2/Al_2O_3 ratios (McLennan et al., 1993), whereby increasing ratios signify increasing textural maturity. SiO_2/Al_2O_3 ratios for mud and silt samples from the BJR vary from 4.79 to 7.37 and are generally higher than in post-Archean average Australian sedimentary rock (PAAS ~3.3). However, the SiO_2/Al_2O_3 ratios of the bar-top samples (6.61–7.68) are relatively higher than the facies samples (6.03–8.69) (Table 2). The plots of SiO_2/Al_2O_3 and major elements such as TiO_2, MgO and P_2O_5, and total Fe oxide (not shown in Fig. 8) show slight relatively decreasing trend in abundance with increase in SiO_2/Al_2O_3. TiO_2, MgO and P_2O_5, and total Fe oxide contents are comparatively lower in abundance in the fine-grained sands, which lie at $SiO_2/Al_2O_3 > 6.0$. Although there is considerable overlap, very fine sands show relatively greater abundances as SiO_2/Al_2O_3 decreases from 7 to 4.7. Silts and muds partially overlap with very fine-grained sands in SiO_2/Al_2O_3, but show some increasing abundances in TiO_2, MgO, P_2O_5, and total Fe content.

In general, the contents of CaO decrease with the increase in SiO_2/Al_2O_3. In contrast, concentrations of Na_2O do not strongly vary (1.5–2%), in samples of fine sand to mud, whereas CaO concentrations in bar-top fine sands (2.15φ) are highly variable (Fig. 8b) but the tendency to decrease with increasing SiO_2/Al_2O_3 is very weak (Fig. 8e). In the studied samples of the BJR, MnO concentrations show no apparent correlation with SiO_2/Al_2O_3 (Fig. 8f).

The results demonstrate that grain size of sediments influences variations in major element contents, suggesting that sorting of particles during transport could lead to preferential enrichment of specific minerals in certain grain-size fractions (Whitemore et al., 2004). The general negative relations of Ti, K and total Fe oxide (not shown in Fig. 8) concentrations with SiO_2/Al_2O_3 values suggest that these elements reside mainly in clay matrix phases (Roser et al., 2000). In the studied sedimentary samples, P_2O_5 may be influenced by the presence of P-bearing accessory minerals, particularly apatite (Roser et al., 2000), as manifested by scatter above (Fig. 8d). On geochemical grounds, MnO should also be concentrated in clays. But in this case, due to mobility in surficial conditions (Roser et al., 2000), MnO data do not show correlation with grain size.

The lack of correlation of Na_2O with SiO_2/Al_2O_3 (Fig. 8e) reflects abundance of plagioclase in sands. Similarly, the feldspar effect can be inferred to some degree from the K_2O plot with SiO_2/Al_2O_3 (Fig. 8c). Although K_2O is largely associated to sediment matrix, K_2O contents in sands are still appreciable (2–3.5 wt.%), though the decrease in their values from mud to sand samples is poorly defined compared to variations in concentrations of other clay-linked elements. This is due to the compensatory effect of abundant K-feldspar in sands. A similar effect is also apparent from tendency of CaO to decrease with SiO_2/Al_2O_3 (Fig. 8b), which is likely due to scarcity of Ca-plagioclase in the samples of sand relative to the samples of mud.

4.3.2. Trace elements

The concentrations of trace elements in the BJR sediment samples (Table 3), except Sr and Nb contents in the upper BJR and Ni, Cr, Sr, Pb and Nb contents in the lower BJR, are similar to those in the UCC (Fig. 9). However, sands show lower values of trace elements concentration in most of the samples relative to the associated silts and muds (Table 3). In contrast, the silt and mud samples are variably enriched in Cr and Th and depleted in Sr, Pb and Nb, indicating a mineralogical (e.g., clays, chlorite, heavy minerals and grain coating) control on sediment geochemistry (Table 3). The depletion of Sr, Pb and Nb is mainly because of dilution effect of silica in silt and mud sediments (Tripathia et al., 2007). Besides, some basic input and sorting effects may play significant role for this enrichment. The Sr contents (134–192 ppm) are variable (standard deviation of ca. 15 ppm) because of the probabilityof many influences on Sr in low temperature depositional environments (Fairbridge, 1972). For example, fractionation of Sr can result from the weathering of feldspars, particularly plagioclase (Rahman and Suzuki, 2007). Considering the fact that the fluvial samples contain some amount of feldspars, with plagioclase as the dominant feldspar component (Table 1), the depletion of Sr in the analyzed sediment samples is likely due to weathering of plagioclase.

Trace element distributions for different grain size are shown in Figs. 10 and 11. In all samples, Rb, Nb, Cr, V, and Y (Fig. 10a–e) slightly decrease as SiO_2/Al_2O_3 increases from muds to fine sands. Due to small sample size of samples of silt and mud, the correlation trend is not clear. Other than such scatter plots, however, the data show some trace element compositional differences depending on grain-size variation. For example, Fig. 10 (a,f) shows that Rb and Th contents are relatively higher in samples of silt and mud, although there is some overlap in the range of Rb and Th contents in the different samples according to grain size. This indicates that these elements Rb and Th may reside in clay-sized detritus. Similarly, Sr to some extent increases with increasing grain size (150 to 175 ppm for fine sands and 130 to150 ppm for very fine sand, silts and muds), albeit with considerable scatter (Fig. 11a). Considering the close geochemical association of Sr with Ca and the extent of non-detrital Ca-enrichment, the strength of the correlation between Ca and Sr is considerable. This implies that Sr is likely associated with Ca in detrital plagioclase (Roser et al., 2000). Barium exhibits no systematic relation with grain size (Fig. 11b). Barium may substitute for K in either micas or feldspars, but more strongly in the latter (Taylor, 1965). Nevertheless, the lack of correlation of Ba with

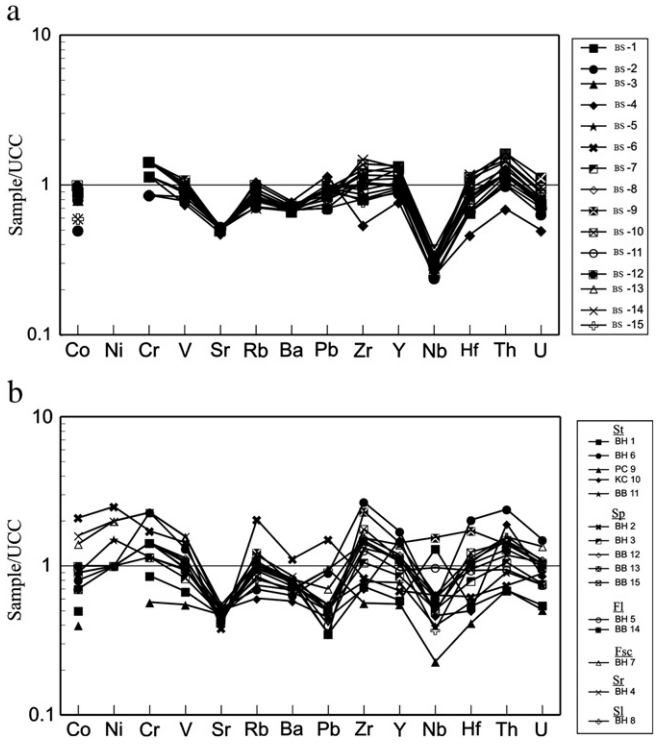

Fig. 9. Multi-element contents of the Brahmaputra–Jamuna River sediment samples, normalized to the upper continental crust (UCC) (Taylor and Mclennan, 1985). (a) Bar-top samples and (b) Facies samples.

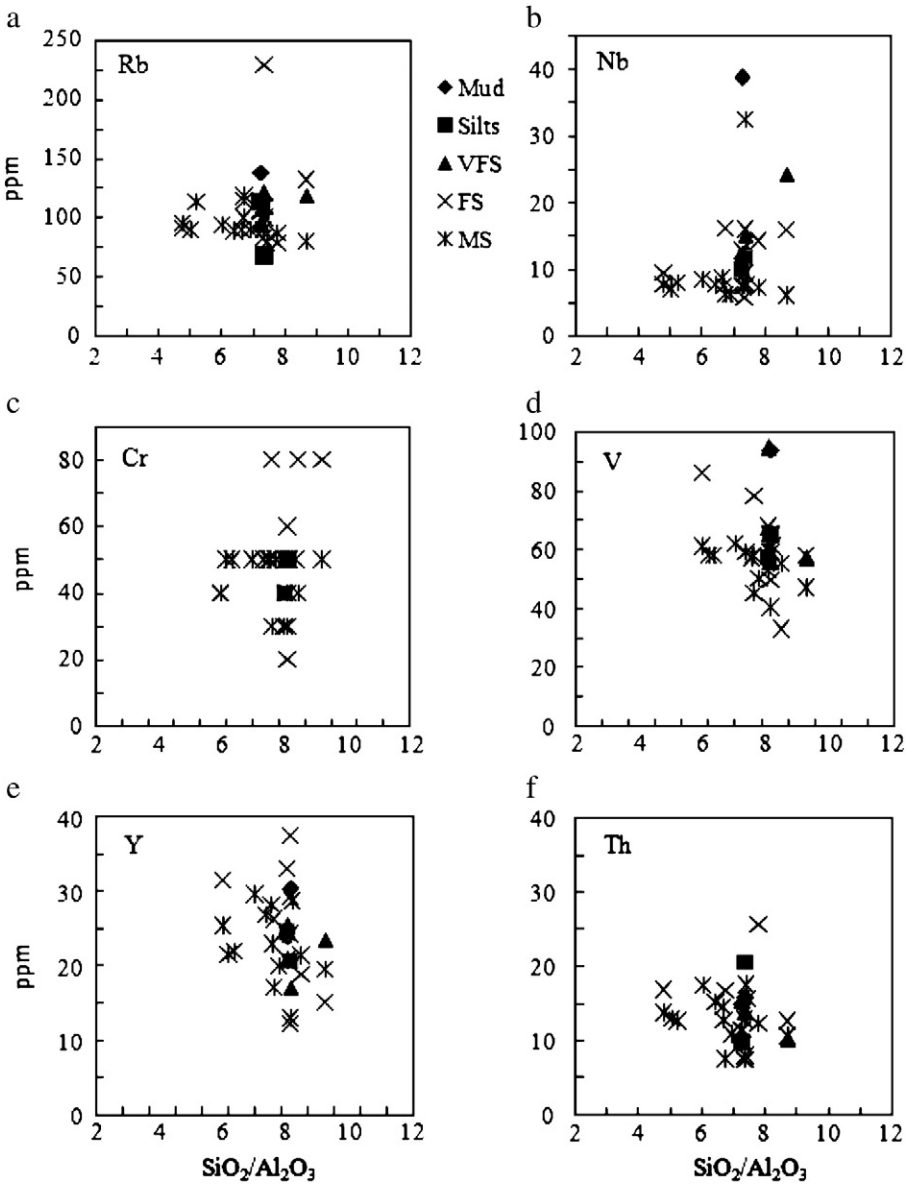

Fig. 10. Trace elements (Rb, Nb, Cr, V, Y and Th) (ppm)-SiO_2/Al_2O_3 variation diagrams, by grain-size class. BFS = bar-top fine sand; FFS = facies fine sand; VFS = very fine sand.

SiO_2/Al_2O_3 is therefore likely due to the compensation effect of varying clay and K-feldspar abundances (Roser et al., 2000). There is poor negative correlation between Zr (Fig. 11c) with SiO_2/Al_2O_3. Zr decreases slightly as grain size increases, but most samples scatter in a broad band between 100 and 400 ppm Zr (Fig. 10e). However, poor negative correlation of Zr with SiO_2/Al_2O_3 suggests residence of Zr in fine-grained detritus, because it typically occurs as the mineral zircon. In addition, few samples show very high (or outlier) values of Zr, indicating zircon concentration.

Four elements (Pb, Ce, Th, and Ga) make identification of the grain-size trends (Fig. 11d–f), where it is clear that Th (Fig. 10f), Ce and Ga (Fig. 11e–f) generally decrease as SiO_2/Al_2O_3 increases. This implies that the presence of clay has some control on elemental concentration (Roser et al., 2000). For Th and Ce, however, some samples (especially for SiO_2/Al_2O_3 values of ca. 6) scatter to higher values. This is characteristic of clays, chlorite, and heavy minerals concentration (Roser et al., 2000). The trend of Ga is particularly clear, which is consistent with the close geochemical association of this element with Al (Fig. 11f). Pb shows a clear trend of decreasing concentration with increasing SiO_2/Al_2O_3 ratio, which indicates a marked grain-size control (Fig. 10d) (Taylor, 1965).

4.3.3. Rare earth elements (REEs)

Compared with their associated silt and mud, sand samples have slightly lower REE contents (Fig. 11). Despite differing REE contents, however, most of the silt and mud and most of the sand samples from, respectively, the upper and lower BJR (bar-top and different facies units) display similar chondrite-normalized REE patterns with some overlapping abundances and a slight negative Eu anomaly (Fig. 12). This result is in agreement with the study of floodplain deposits of southern India by Singh and Rajamani (2001a) and Rahman and Suzuki (2007) on Miocene sediments of BB. The average concentrations of REEs decrease from the upstream bar-top fine-grained sands to the downstream sedimentary facies units (very fine sands, silts and muds). The two groups of sediments in this study (i.e., bar-top and sedimentary facies) show fractionated, parallel to sub-parallel REE patterns, with $(La/Yb)_N$ ratios ranging between 8.14 and 13.3 (Tables 2 and 4), with mean of 10.00. The composition of both LREEs and HREEs in the studied samples shows variable fractionation with $(La/Sm)_N$ values ranging between 3.92 and 5.3 with mean of 4.3. Furthermore, $(Gd/Yb)_N$ values range between 0.98 and 1.80 with mean of 1.57. However, all the samples demonstrate consistent homogeneous negative Eu anomalies (Eu/Eu^*) with values ranging between 0.51

and 0.83 with mean of 0.66. This implies that the negative Eu anomaly observed in the sediments is likely representative of their source-rock characteristics.

4.3.4. Correlation

The compositional variations in Al_2O_3, TiO_2, FeO, MgO, MnO, Cr and Co, are due to variations in the concentrations of silica that ranges between 65 and 80% are reflected in strong to moderate negative correlations between silica and the former elements (Tables 5a–c). In the bar-top samples, the correlation coefficients of the oxide pairs are −0.77 for SiO_2–Al_2O_3, −0.63 for SiO_2–TiO_2, −0.88 for SiO_2– Fe_2O_3 (T), −0.86 for SiO_2–MgO, −0.62 for SiO_2–MnO, −0.68 for SiO_2–K_2O, −0.73 for SiO_2–Be, −0.72 for SiO_2–V, −0.80 for SiO_2–Cr, −0.74 for SiO_2–Co, −0.60 for SiO_2–Nb, −0.61 for SiO_2–Cs, −0.50 for SiO_2–Hf and −0.51 for SiO_2–U (Table 5a). In contrast, CaO, Na_2O, K_2O, Sr, Ni, Th and Zr show no significant correlation with silica, whereas Al_2O_3 shows no significant correlation with most elements except Fe_2O_3 (T), Co and Cs (Table 4a). In the facies samples (Table 5b), the correlation coefficients between SiO_2 and the major elements are similar to that of bar-top samples; but, Al_2O_3 shows moderate to poor positive correlations with TiO_2 (0.69), Fe_2O_3 (0.92), MnO (0.61), MgO (0.90), K_2O (0.66), Be (0.66), Sc (0.59), V (0.79), Cr (0.61), Co (0.96), Cs (0.78) and Ba (0.85). However, the combination of bar-top and facies samples (Table 5c) shows that silica is negatively correlated with major oxides and some trace elements such as Be (−0.73), V(−0.90), Cr (−0.78), Co (−0.93), Cs (−0.66) and Ba (−0.71). Al_2O_3 shows moderate to poor correlation with all elements in all samples except Na_2O, CaO, and P_2O_5. On the other hand, most of the trace and rare earth elements show no significant correlation except Be, V, Cr, Co, Cs and Ba (Table 5c).

Strong positive correlations of K with Al, Cs, Ba, total REE, Th and U suggest that the concentrations of these trace elements are controlled by alumino-phyllosilicates (mainly clay minerals and mica) (McLennan and Taylor, 1983; Rahman and Suzuki, 2007). In the present study, a significant correlation coefficient (0.96) between Ba and K_2O suggests that Ba is mainly associated with feldspar components. High-field strength elements (e.g., Zr, Nb, Hf, Y) generally show consistent inter-relationships with the ferromagnesian trace elements (Cr, Ni, V, Co, and Sc) (Rahman and Suzuki, 2007). These relationships among HFSEs and ferromagnesian element demonstrate the chemical coherence and uniformity of fluvial sediments. However, grain size and sorting play significant role on chemical coherence and uniformity of the sediments.

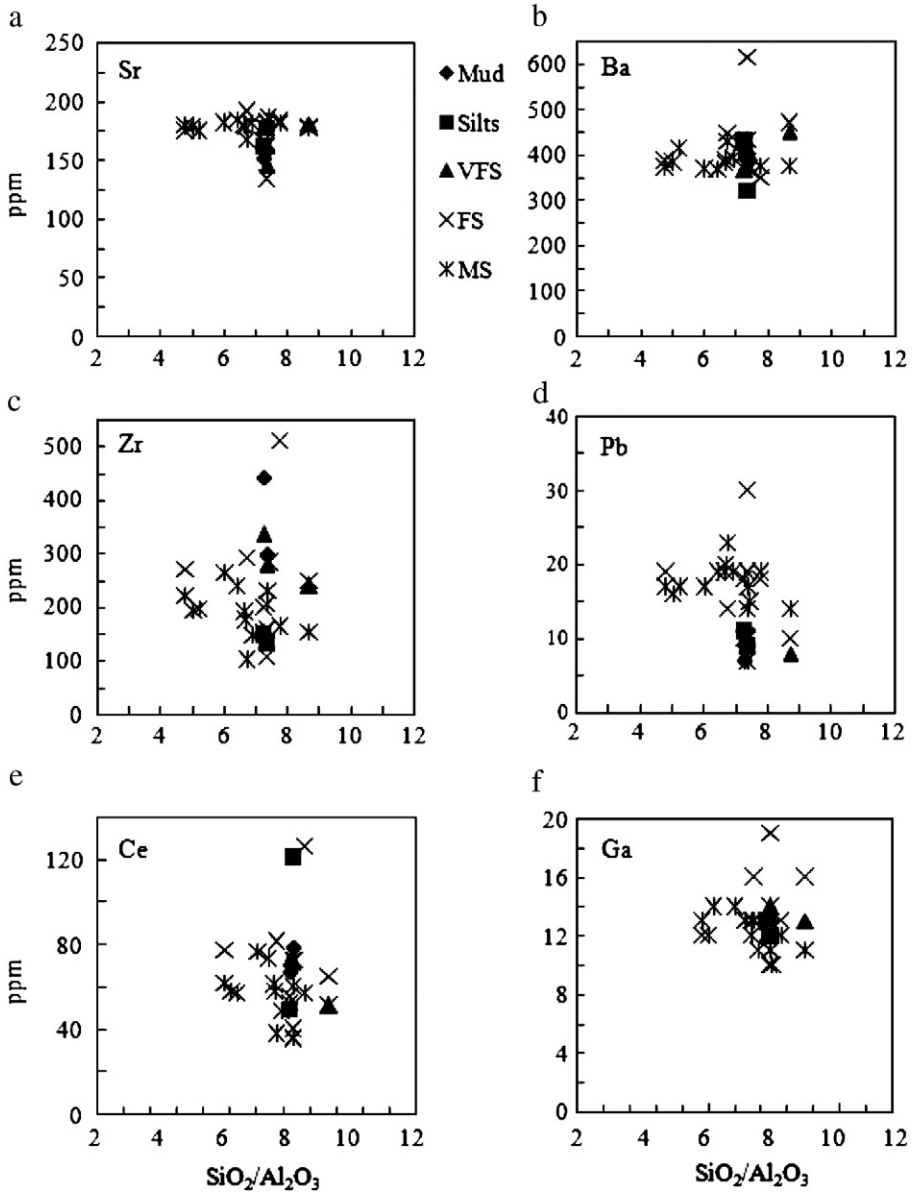

Fig. 11. Trace elements (Sr, Ba, Zr, Pb, Ce and Ga) (ppm)-SiO_2/Al_2O_3 variation diagrams, by grain-size class. BFS = bar-top fine sand; FFS = facies fine sand; VFS = very fine sand.

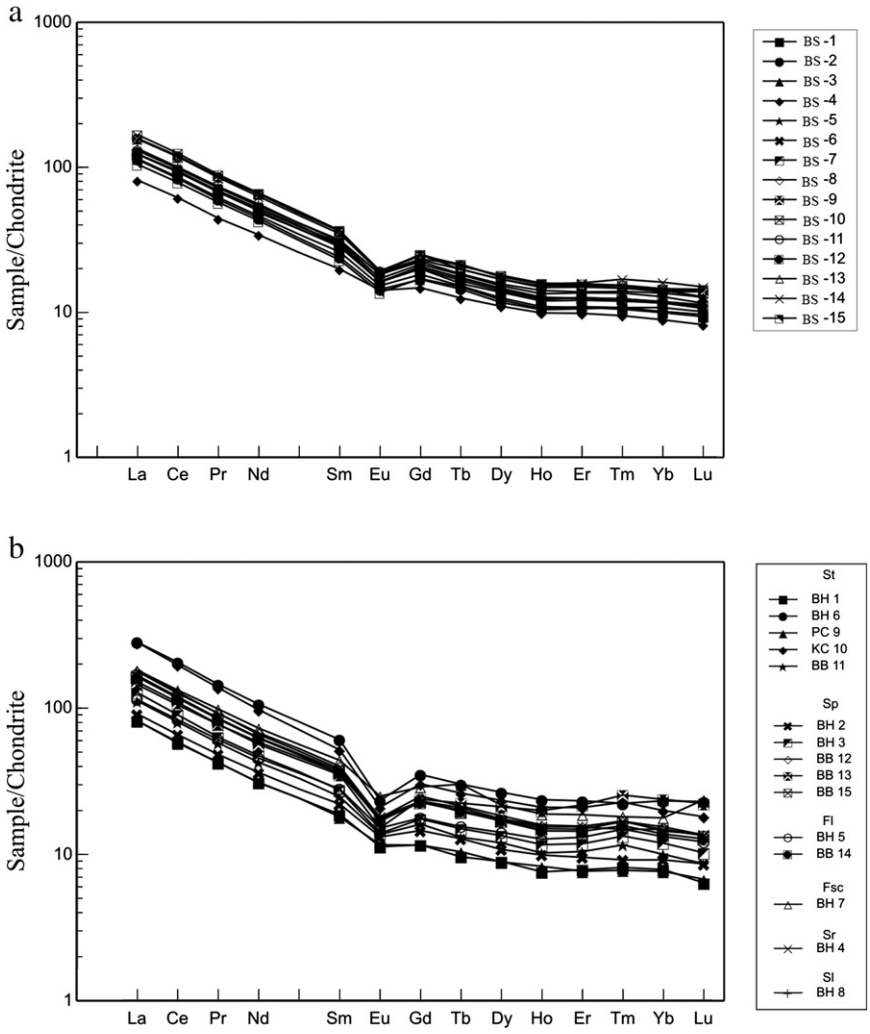

Fig. 12. Patterns of chondrite-normalized rare earth elements (REE) in the Brahmaputra–Jamuna River sediment samples. Chondrite values from Taylor and McLennan (1985). (a) Bar-top samples and (b) facies samples.

In the present study, Co and Sc abundances show significant positive correlations with Ni, V and Al_2O_3, suggesting that Co and Sc are partly controlled by accessory non-aluminous silicate minerals (Rahman and Suzuki, 2007).

The high correlation coefficients between Fe and Ti (0.86), Fe and Mg (0.89), Fe and Mn (0.84), and Ti and Mg (0.85) indicate that these elements likely reside in similar mineral phases, probably biotite, muscovite and garnet. Poor or lack of correlations between Th, P_2O_5, Zr and Y suggest, however, that Th is not controlled dominantly by single mineral (e.g., zircon, clays, apatite or monazite), but more likely by a combination of minerals (Condie, 1991).

4.3.5. Sorting and maturation

In the QFL diagram (Fig. 5), all the analyzed samples plot together with no significant variation in the tectonic provenance field of recycled orogen, which has been defined as deformed and uplifted, dominantly sedimentary strata (Dickinson, 1985).

Slight differences in the plots of the samples (sand in the upper BJR and silt and mud in the lower BJR) reflect variations in concentrations of quartz relative to feldspar, due to combined effects of weathering and mechanical disintegration. Moreover, the quartz enrichment was quite apparent on the SiO_2/Al_2O_3 plots (Figs. 8 and 10). Due to the effect of sorting, all the sediment samples plot close to the Q–F line (Fig. 5). This

Table 4
Ranges of elemental ratios of Brahmaputra–Jamuna fluvial sediments in this study compared to elemental rations in sediments derived from the Surma Group of Bengal Basin, felsic rocks, mafic rocks and in the upper continental crust (UCC).

Elemental ratios	Bar-top sediments (n = 15)	Facies units sediments (n = 15)	Surma Group sandstones [a]	Ranges in sediments from felsic sources[b]	Ranges in sediments from mafic sources[b]	Upper continental crust [c]
Eu/Eu*	0.51–0.80	0.62–0.83	0.63–0.77	0.40–0.94	0.71–0.95	0.63
La/LuN	6.57–15.13	9.59–11.91	7.65–11.28	3.00–27.0	1.10–7.00	9.73
La/Sc	1.97–6.26	2.76–3.98	2.89–5.01	2.50–16.3	0.43–0.86	2.21
Th/Sc	0.72–2.33	1.06–1.75	0.85–2.17	0.84–20.5	0.05–0.22	0.79
La/Co	1.03–9.56	2.41–6.2	1.09–7.65	1.80–13.8	0.14–0.38	1.76
Th/Co	0.38–2.93	0.93–2.6	0.41–3.25	0.04–3.25	0.04–1.40	0.63
Cr/Th	2.44–7.59	2.78–5.38	4.92–19.77	4.00–15.00	25–500	7.76

[a] Rahman and Suzuki (2007).
[b] Cullers et al. (1988); Cullers (1994, 2000); Cullers and Podkovyrov (2000).
[c] McLennan (2001); Taylor and McLennan (1985).

Table 5a
Correlation matrix of bar-top samples of the Brahmaputra–Jamuna River sediments. Underscores of coefficients indicate significant (+) correlation and (−) correlations are denoted by bolds.

	SiO_2	Al_2O_3	TiO_2	Fe_2O_3	MnO	MgO	CaO	Na_2O	K_2O	P_2O_5	CIA	Be	V	Cr	Co	Br	Y	Zr	Nb	Cs
SiO_2	1.00																			
Al_2O_3	**−0.77**	1.00																		
	0.00																			
TiO_2	**−0.63**	0.22	1.00																	
	0.01	0.43																		
Fe_2O_3	**−0.88**	0.55	0.90	1.00																
	0.00	0.03	0.00																	
MnO	**−0.62**	0.26	0.93	0.89	1.00															
	0.01	0.35	0.00	0.00																
MgO	**−0.86**	0.49	0.91	0.96	0.80	1.00														
	0.00	0.06	0.00	0.00	0.00															
CaO	−0.30	−0.19	0.89	0.65	0.76	0.71	1.00													
	0.28	0.51	0.00	0.01	0.00	0.00														
Na_2O	0.38	0.07	−0.38	−0.43	−0.47	−0.34	−0.22	1.00												
	0.16	0.81	0.16	0.11	0.08	0.22	0.43													
K_2O	−0.11	0.39	**−0.58**	−0.27	−0.50	−0.29	**−0.82**	−0.14	1.00											
	0.69	0.15	0.02	0.34	0.06	0.29	0.00	0.63												
P_2O_5	**−0.68**	0.30	0.86	0.85	0.72	0.91	0.73	−0.40	−0.29	1.00										
	0.01	0.27	0.00	0.00	0.00	0.00	0.00	0.15	0.29											
CIA	−0.01	0.08	−0.06	0.06	0.02	0.00	−0.18	−0.28	0.41	0.27	1.00									
	0.99	0.78	0.83	0.83	0.94	1.00	0.52	0.31	0.13	0.34										
Be	**−0.56**	0.02	0.92	0.80	0.82	0.85	0.92	−0.42	**−0.61**	0.84	−0.11	1.00								
	0.03	0.95	0.00	0.00	0.00	0.00	0.00	0.12	0.02	0.00	0.69									
V	**−0.72**	0.27	0.97	0.92	0.87	0.96	0.85	−0.41	−0.45	0.92	0.03	0.93	1.00							
	0.00	0.34	0.00	0.00	0.00	0.00	0.00	0.13	0.10	0.00	0.91	0.00								
Cr	**−0.80**	0.50	0.83	0.92	0.78	0.88	0.56	−0.49	−0.21	0.85	0.13	0.75	0.83	1.00						
	0.00	0.06	0.00	0.00	0.00	0.00	0.03	0.06	0.46	0.00	0.63	0.00	0.00							
Co	**−0.74**	0.65	0.34	0.62	0.24	0.66	0.06	−0.25	0.36	0.62	0.39	0.32	0.50	0.66	1.00					
	0.00	0.01	0.22	0.02	0.39	0.01	0.82	0.38	0.19	0.01	0.16	0.25	0.06	0.01						
Br	−0.12	−0.25	0.72	0.46	0.61	0.53	0.92	0.06	**−0.88**	0.54	−0.30	0.78	0.67	0.30	0.66	1.00				
	0.67	0.37	0.00	0.09	0.02	0.04	0.00	0.84	0.00	0.04	0.27	0.00	0.01	0.28	0.61					
Y	−0.41	0.04	0.91	0.72	0.80	0.76	0.87	−0.30	**−0.59**	0.75	−0.12	0.86	0.86	0.69	0.21	0.73	1.00			
	0.13	0.88	0.00	0.00	0.00	0.00	0.00	0.27	0.02	0.00	0.68	0.00	0.00	0.00	0.45	0.00				
Zr	−0.49	0.04	0.92	0.76	0.88	0.77	0.89	−0.39	**−0.66**	0.70	−0.24	0.91	0.86	0.69	0.13	0.77	0.90	1.00		
	0.06	0.89	0.00	0.00	0.00	0.00	0.00	0.15	0.01	0.00	0.38	0.00	0.00	0.01	0.64	0.00	0.00			
Nb	**−0.60**	0.34	0.82	0.80	0.71	0.83	0.63	−0.34	−0.23	0.77	0.11	0.69	0.84	0.73	0.56	0.44	0.85	0.65	1.00	
	0.02	0.22	0.00	0.00	0.00	0.00	0.01	0.22	0.40	0.00	0.71	0.00	0.00	0.00	0.03	0.10	0.00	0.01		
Cs	**−0.61**	0.82	−0.13	0.27	−0.07	0.23	−0.50	−0.14	**0.80**	0.12	0.32	−0.23	0.01	0.24	0.72	**−0.59**	−0.26	−0.28	0.16	1.00
	0.02	0.00	0.65	0.34	0.80	0.41	0.06	0.62	0.00	0.66	0.25	0.41	0.98	0.38	0.00	0.02	0.36	0.32	0.57	

	SiO_2	Al_2O_3	TiO_2	Fe_2O_3	MnO	MgO	CaO	Na_2O	K_2O	P_2O_5	CIA	Be	V	Cr	Co	Br	Y	Zr
Ba	−0.05	0.57	**−0.64**	−0.31	−0.50	−0.40	**−0.91**	0.20	0.82	−0.49	0.22	**−0.76**	**−0.60**	−0.26	0.21	**−0.87**	**−0.70**	**−0.71**
	0.85	0.03	0.01	0.26	0.06	0.14	0.00	0.47	0.00	0.07	0.44	0.00	0.02	0.34	0.46	0.00	0.00	0.00
Hf	**−0.51**	0.07	0.90	0.76	0.85	0.77	0.86	−0.41	**−0.60**	0.71	−0.25	0.90	0.86	0.68	0.16	0.75	0.89	0.99
	0.05	0.79	0.00	0.00	0.00	0.00	0.00	0.13	0.02	0.00	0.37	0.00	0.00	0.01	0.56	0.00	0.00	0.00
Pb	0.07	0.33	−0.42	−0.25	−0.42	−0.23	**−0.55**	0.31	0.58	−0.18	0.22	−0.49	−0.36	−0.11	0.20	**−0.51**	−0.30	**−0.50**
	0.81	0.23	0.12	0.38	0.12	0.41	0.04	0.26	0.02	0.51	0.44	0.07	0.19	0.69	0.47	0.05	0.28	0.06
Th	−0.45	0.02	0.92	0.74	0.80	0.80	0.90	−0.35	**−0.59**	0.78	−0.10	0.88	0.91	0.66	0.25	0.76	0.96	0.91
	0.09	0.95	0.00	0.00	0.00	0.00	0.00	0.20	0.02	0.00	0.71	0.00	0.00	0.01	0.37	0.00	0.00	0.00
U	**−0.51**	0.09	0.88	0.75	0.78	0.81	0.83	−0.36	−0.46	0.78	−0.04	0.84	0.90	0.59	0.30	0.74	0.91	0.84
	0.05	0.76	0.00	0.00	0.00	0.00	0.00	0.19	0.09	0.00	0.88	0.00	0.00	0.02	0.28	0.00	0.00	0.00
La	−0.39	−0.07	0.90	0.70	0.79	0.75	0.92	−0.38	**−0.65**	0.74	−0.16	0.90	0.87	0.64	0.19	0.80	0.94	0.94
	0.15	0.80	0.00	0.00	0.00	0.00	0.00	0.17	0.01	0.00	0.58	0.00	0.00	0.01	0.51	0.00	0.00	0.00
Ce	−0.41	−0.06	0.90	0.71	0.80	0.76	0.92	−0.39	**−0.65**	0.76	−0.16	0.91	0.88	0.66	0.19	0.80	0.93	0.95
	0.13	0.84	0.00	0.00	0.00	0.00	0.00	0.16	0.01	0.00	0.58	0.00	0.00	0.01	0.49	0.00	0.00	0.00
Nd	−0.45	−0.03	0.92	0.74	0.80	0.79	0.92	−0.41	**−0.62**	0.80	−0.13	0.93	0.90	0.69	0.24	0.79	0.93	0.94
	0.10	0.91	0.00	0.00	0.00	0.00	0.00	0.13	0.01	0.00	0.64	0.00	0.00	0.00	0.40	0.00	0.00	0.00
S	−0.50	0.02	0.94	0.79	0.82	0.83	0.92	−0.41	**−0.61**	0.82	−0.12	0.94	0.92	0.76	0.30	0.76	0.93	0.93
	0.06	0.95	0.00	0.00	0.00	0.00	0.00	0.13	0.02	0.00	0.67	0.00	0.00	0.00	0.27	0.00	0.00	0.00
Eu	**−0.52**	0.09	0.92	0.80	0.82	0.82	0.85	−0.43	**−0.53**	0.79	−0.13	0.90	0.88	0.81	0.34	0.65	0.94	0.89
	0.05	0.74	0.00	0.00	0.00	0.00	0.00	0.11	0.04	0.00	0.65	0.00	0.00	0.00	0.21	0.01	0.00	0.00
Gd	**−0.51**	0.07	0.94	0.79	0.79	0.85	0.90	−0.37	**−0.59**	0.84	−0.12	0.93	0.92	0.78	0.34	0.74	0.95	0.91
	0.05	0.81	0.00	0.00	0.00	0.00	0.00	0.18	0.02	0.00	0.67	0.00	0.00	0.00	0.21	0.00	0.00	0.00
Dy	**−0.51**	0.11	0.95	0.80	0.84	0.83	0.88	−0.36	**−0.58**	0.81	−0.11	0.90	0.91	0.79	0.29	0.72	0.98	0.92
	0.05	0.71	0.00	0.00	0.00	0.00	0.00	0.19	0.02	0.00	0.69	0.00	0.00	0.00	0.30	0.00	0.00	0.00
Yb	−0.39	−0.02	0.92	0.72	0.86	0.72	0.90	−0.35	**−0.70**	0.67	−0.23	0.89	0.83	0.70	0.08	0.76	0.95	0.95
	0.15	0.95	0.00	0.00	0.00	0.00	0.00	0.20	0.00	0.01	0.41	0.00	0.00	0.00	0.79	0.00	0.00	0.00
Lu	−0.41	−0.02	0.91	0.72	0.84	0.73	0.89	−0.40	**−0.64**	0.71	−0.20	0.90	0.85	0.68	0.11	0.76	0.96	0.96
	0.13	0.94	0.00	0.00	0.00	0.00	0.00	0.14	0.01	0.00	0.49	0.00	0.00	0.01	0.69	0.00	0.00	0.00

Table 5a (*continued*)

Nb	Cs	Ba	Hf	Pb	Th	U	La	Ce	Nd	S	Eu	Gd	Dy	Yb	Lu
−0.39	0.75	1.00													
0.15	0.00														
0.67	−0.20	**−0.67**	1.00												
0.01	0.47	0.01													
−0.12	0.48	0.56	−0.43	1.00											
0.68	0.07	0.03	0.11												
0.85	−0.23	**−0.73**	0.91	−0.37	1.00										
0.00	0.42	0.00	0.00	0.17											
0.87	−0.09	**−0.65**	0.86	−0.35	0.96	1.00									
0.00	0.75	0.01	0.00	0.20	0.00										
0.76	−0.30	**−0.78**	0.95	−0.41	0.98	0.92	1.00								
0.00	0.28	0.00	0.00	0.13	0.00	0.00									
0.75	−0.29	**−0.78**	0.96	−0.41	0.97	0.91	1.00	1.00							
0.00	0.29	0.00	0.00	0.13	0.00	0.00	0.00								
0.77	−0.26	**−0.77**	0.95	−0.38	0.97	0.92	0.99	1.00	1.00						
0.00	0.35	0.00	0.00	0.16	0.00	0.00	0.00	0.00							
0.79	−0.23	**−0.75**	0.93	−0.36	0.96	0.90	0.98	0.98	0.99	1.00					
0.00	0.42	0.00	0.00	0.19	0.00	0.00	0.00	0.00	0.00						
0.82	−0.16	**−0.67**	0.90	−0.25	0.91	0.85	0.92	0.93	0.94	0.96	1.00				
0.00	0.57	0.01	0.00	0.38	0.00	0.00	0.00	0.00	0.00	0.00					
0.83	−0.19	**−0.72**	0.91	−0.30	0.96	0.90	0.96	0.97	0.98	0.99	0.97	1.00			
0.00	0.49	0.00	0.00	0.28	0.00	0.00	0.00	0.00	0.00	0.00	0.00				
0.84	−0.20	**−0.68**	0.91	−0.28	0.96	0.89	0.95	0.95	0.96	0.97	0.97	0.98	1.00		
0.00	0.47	0.01	0.00	0.31	0.00	0.00	0.00	0.00	0.00	0.00	0.00	0.00			
0.70	−0.37	**−0.74**	0.93	−0.42	0.89	0.81	0.92	0.92	0.91	0.92	0.94	0.92	0.95	1.00	
0.00	0.17	0.00	0.00	0.12	0.00	0.00	0.00	0.00	0.00	0.00	0.00	0.00	0.00		
0.73	−0.31	**−0.73**	0.96	−0.36	0.94	0.87	0.96	0.96	0.96	0.95	0.95	0.95	0.97	0.98	1.00
0.00	0.27	0.00	0.00	0.19	0.00	0.00	0.00	0.00	0.00	0.00	0.00	0.00	0.00	0.00	

provides best indication of the bulk source-rock composition, which is felsic.

4.4. Provenance and tectonic setting

4.4.1. Major elements

Among all schemes to determine provenance and tectonic setting of deposition of sedimentary suites, the scheme discussed by Roser and Korsch (1988) provides a convenient method of viewing stratigraphic variation among sample suites. In the discriminant function diagram of Roser and Korsch (1988), all the samples fall within the recycled-mature polycyclic quartzose detritus field (Fig. 13), but the bar-top fine-sand samples closer to the boundary of felsic igneous provenance. However, this pattern is consistent with derivation from a felsic source terrane, with superimposed sedimentary maturation or weathering (Roser et al., 2000). Recycled sources characterize quartzose sediments of mature continental provenance, and the origin of the sediments is likely from a highly weathered granite-gneiss terrain and/or from a pre-existing sedimentary terrain as in the case of the southern Himalayas (Rahman and Suzuki, 2007; Singh, 2010). The recycled nature of the BJR sediments is also reflected in the sandstone modal compositional QFL diagram (Fig. 5). Similar results were obtained for Miocene Surma Group sandstones in the BB by Rahman and Suzuki (2007). Thus, the sediments of the BJR in the BB have dominantly quartzolithic composition with predominance of quartz, abundant low-grade metamorphic and sedimentary lithics, less feldspars and little volcanic detritus

In the bivariate tectonic discrimination diagram of Roser and Korsch (1986), the sediment samples of BJR plot astride the ACM and PM field with most samples clustering at the boundary separating the two fields (Fig. 14). Some fine sand samples of bar-top and trough-cross bed sediments fall in the PM field, whereas most fine-grained facies samples (very fine sand, silts and muds) plot in the active continental margin (ACM) field (Fig. 14). This plot indicates that rocks that developed in both passive and active continental margins are the main sources of the BJR sediments. However, fine-sand samples of bar-top sediments contain more SiO_2, whereas the ratio Na_2O/K_2O is higher in the silt and mud facies samples. High Na_2O/K_2O ratio and low SiO_2 content in some of the samples plot them in the ACM margin field. Thus, the tectonic discrimination diagrams must be used with some constraints. Most of the samples that plot within the PM field are dominated by quartz-rich sediments and rest fall in the ACM field, reflecting more weathered material (e.g., mud). This interpretation is supported by the provenance discrimination diagram of Roser and Korsch (1988), which shows that the samples represent a recycled-mature polycyclic quartzose sedimentary provenance (Fig. 13).

Based on oxide composition data, Bhatia (1983) proposed discrimination diagrams for tectonic settings including oceanic island arc, continental island arc, active continental margin and passive margin settings. Most of the samples in this study fall in the active continental margin field in the diagrams of $(Fe_2O_3 + MgO)$ versus Al_2O_3/SiO_2, K_2O/Na_2O, $Al_2O_3/(CaO + Na_2O)$, TiO_2 and Al_2O_3/SiO_2 (Fig. 15). However, there are some scatter on some of the plots and few samples plot close to the continental island arc margin field (Fig. 15). All the fine-sand samples of bar-top sediments fall within the active continental margin, whereas some of the very fine sand, silt and mud samples of the facies sediments plot close to the continental island arc. Thus, some of the facies samples plot close to the continental island arc field whereas most of the samples fall in the ACM field.

4.4.2. Trace elements

The mean concentrations (in ppm) of Rb (~104), Sr (~173), Sm (~4.94) and Nd (~26) in the BJR sands are consistent with those in the Upper Himalaya sedimentary series (France-Lanord et al., 1993). The values of Eu/Eu*, $(La/Lu)_N$, La/Sc, Th/Sc, La/Co, Th/Co and Cr/Th in this study are more similar to values for sediments derived from felsic source rocks than to those for mafic source rocks (Table 3), thus suggesting that they likely originated from felsic rocks. Furthermore, the elevated LREE/HREE ratios and negative Eu anomalies of the BJR sediments (Table 4) bear the characteristics of felsic source rocks (after Taylor and McLennan, 1985; Wronkiewicz and Condie, 1989). In the $(Eu/Eu^*)_N$ vs. Gd_N/Yb_N diagram (Fig. 16), all the samples of sediments from the BJR plot in the field of Gd_N/Yb_N ratio <2 and

Table 5b
Correlation matrix of the facies samples of the Brahmaputra–Jamuna River sediments. Underscores of coefficients indicate significant (+) correlation and (−) correlations are denoted by bolds.

	SiO_2	Al_2O_3	TiO_2	Fe_2O_3	MnO	MgO	CaO	Na_2O	K_2O	P_2O_5	CIA	Be	V	Cr	Co	Br	Y	Zr	Nb	Cs	Ba
SiO_2	1.00																				
Al_2O_3	**−0.96**	1.00																			
	0.00																				
TiO_2	**−0.83**	0.69	1.00																		
	0.00	0.00																			
Fe_2O_3	**−0.95**	0.92	0.85	1.00																	
	0.00	0.00	0.00																		
MnO	**−0.72**	0.61	0.87	0.85	1.00																
	0.00	0.02	0.00	0.00																	
MgO	**−0.96**	0.90	0.84	0.88	0.69	1.00															
	0.00	0.00	0.00	0.00	0.00																
CaO	−0.15	−0.08	0.57	0.11	0.42	0.33	1.00														
	0.61	0.77	0.03	0.69	0.12	0.24															
Na_2O	0.24	−0.22	−0.27	−0.48	**−0.60**	−0.17	0.09	1.00													
	0.38	0.44	0.34	0.07	0.02	0.54	0.75														
K_2O	**−0.66**	0.80	0.22	0.66	0.28	0.48	**−0.63**	−0.27	1.00												
	0.01	0.00	0.43	0.01	0.32	0.07	0.01	0.33													
P_2O_5	**−0.58**	0.40	0.87	0.64	0.72	0.61	0.63	−0.26	−0.03	1.00											
	0.02	0.14	0.00	0.01	0.00	0.02	0.01	0.34	0.91												
CIA	−0.33	0.24	0.29	0.21	0.04	0.39	0.18	−0.01	0.02	0.16	1.00										
	0.23	0.38	0.29	0.45	0.90	0.15	0.53	0.96	0.94	0.58											
Be	**−0.80**	0.66	0.96	0.84	0.92	0.84	0.60	−0.40	0.18	0.82	0.23	1.00									
	0.00	0.01	0.00	0.00	0.00	0.00	0.02	0.14	0.52	0.00	0.41										
V	**−0.90**	0.79	0.98	0.92	0.89	0.91	0.48	−0.35	0.35	0.80	0.29	0.97	1.00								
	0.00	0.00	0.00	0.00	0.00	0.00	0.07	0.21	0.20	0.00	0.30	0.00									
Cr	**−0.78**	0.61	0.97	0.78	0.83	0.81	0.62	−0.22	0.14	0.85	0.30	0.94	0.94	1.00							
	0.00	0.02	0.00	0.00	0.00	0.00	0.02	0.44	0.62	0.00	0.28	0.00	0.00								
Co	**−0.94**	0.96	0.73	0.97	0.74	0.85	−0.08	−0.45	0.79	0.50	0.15	0.72	0.83	0.65	1.00						
	0.00	0.00	0.00	0.00	0.00	0.00	0.79	0.10	0.00	0.06	0.58	0.00	0.00	0.01							
Br	−0.03	−0.15	0.29	−0.10	0.09	0.19	0.81	0.43	−0.53	0.29	0.10	0.26	0.24	0.38	−0.21	1.00					
	0.92	0.60	0.29	0.74	0.76	0.51	0.00	0.11	0.04	0.29	0.73	0.35	0.38	0.17	0.45						
Y	−0.19	−0.03	0.64	0.23	0.59	0.28	0.83	−0.14	−0.48	0.74	0.14	0.66	0.51	0.68	0.04	0.45	1.00				
	0.50	0.92	0.01	0.40	0.02	0.31	0.00	0.63	0.07	0.00	0.63	0.01	0.05	0.01	0.90	0.09					
Zr	−0.16	0.01	0.51	0.16	0.29	0.15	0.45	0.14	−0.26	0.65	0.27	0.39	0.34	0.56	0.02	0.19	0.75	1.00			
	0.56	0.98	0.05	0.57	0.29	0.59	0.09	0.63	0.36	0.01	0.34	0.15	0.22	0.03	0.95	0.50	0.00				
Nb	−0.16	0.20	−0.01	0.03	−0.03	0.10	−0.20	0.22	0.23	−0.21	0.25	−0.04	−0.04	0.03	0.05	−0.16	0.08	0.29	1.00		
	0.56	0.48	0.97	0.91	0.92	0.74	0.47	0.43	0.41	0.46	0.36	0.90	0.89	0.91	0.87	0.57	0.78	0.30			
Cs	**−0.66**	0.78	0.34	0.75	0.48	0.47	−0.54	−0.52	0.94	0.15	−0.05	0.33	0.45	0.24	0.85	**−0.60**	−0.31	−0.16	0.11	1.00	
	0.01	0.00	0.22	0.00	0.07	0.08	0.04	0.05	0.00	0.60	0.85	0.23	0.09	0.39	0.00	0.02	0.27	0.57	0.70		

	SiO_2	Al_2O_3	TiO_2	Fe_2O_3	MnO	MgO	CaO	Na_2O	K_2O	P_2O_5	CIA	Be	V	Cr	Co	Br	Y	Zr
Ba	**−0.71**	0.85	0.27	0.69	0.30	0.54	**−0.57**	−0.23	0.99	0.00	0.07	0.23	0.41	0.19	0.82	−0.45	−0.47	−0.26
	0.00	0.00	0.32	0.00	0.28	0.04	0.03	0.41	0.00	0.99	0.81	0.42	0.13	0.49	0.00	0.09	0.08	0.35
Hf	−0.16	0.01	0.51	0.16	0.30	0.15	0.44	0.14	−0.25	0.65	0.24	0.38	0.34	0.56	0.02	0.21	0.74	1.00
	0.56	0.98	0.05	0.57	0.28	0.61	0.10	0.61	0.38	0.01	0.39	0.16	0.22	0.03	0.95	0.46	0.00	0.00
Pb	−0.24	0.28	0.20	0.42	0.32	0.08	−0.29	−0.50	0.49	0.31	−0.31	0.13	0.26	0.13	0.46	−0.26	−0.20	−0.10
	0.39	0.32	0.48	0.12	0.24	0.77	0.29	0.06	0.07	0.26	0.26	0.63	0.36	0.66	0.08	0.36	0.48	0.72
Th	0.01	−0.23	0.53	0.09	0.50	0.07	0.82	−0.17	−0.60	0.69	0.03	0.53	0.38	0.56	−0.12	0.48	0.93	0.69
	0.96	0.41	0.04	0.76	0.06	0.82	0.00	0.56	0.02	0.00	0.92	0.04	0.17	0.03	0.66	0.07	0.00	0.00
U	−0.44	0.26	0.83	0.49	0.64	0.48	0.68	−0.14	−0.17	0.92	0.26	0.75	0.71	0.83	0.32	0.35	0.83	0.80
	0.10	0.35	0.00	0.06	0.01	0.07	0.01	0.61	0.56	0.00	0.35	0.00	0.00	0.00	0.25	0.20	0.00	0.00
La	0.04	−0.25	0.48	0.08	0.54	0.06	0.83	−0.27	−0.62	0.62	−0.05	0.55	0.36	0.51	−0.12	0.46	0.90	0.53
	0.89	0.37	0.07	0.77	0.04	0.85	0.00	0.33	0.01	0.01	0.87	0.04	0.18	0.05	0.66	0.09	0.00	0.04
Ce	0.02	−0.23	0.51	0.10	0.55	0.08	0.83	−0.26	−0.61	0.64	−0.03	0.56	0.38	0.54	−0.11	0.47	0.91	0.55
	0.95	0.41	0.05	0.72	0.03	0.79	0.00	0.36	0.02	0.01	0.91	0.03	0.16	0.04	0.70	0.08	0.00	0.03
Nd	−0.04	−0.18	0.56	0.15	0.57	0.14	0.86	−0.24	−0.59	0.69	0.00	0.61	0.44	0.59	−0.06	0.49	0.92	0.58
	0.88	0.53	0.03	0.60	0.03	0.63	0.00	0.40	0.02	0.00	0.99	0.02	0.10	0.02	0.82	0.06	0.00	0.02
S	−0.11	−0.11	0.63	0.20	0.59	0.20	0.87	−0.20	−0.55	0.75	0.07	0.65	0.49	0.65	−0.02	0.51	0.95	0.66
	0.70	0.69	0.01	0.48	0.02	0.47	0.00	0.48	0.03	0.00	0.79	0.01	0.06	0.01	0.96	0.06	0.00	0.01
Eu	−0.33	0.13	0.76	0.36	0.63	0.46	0.91	−0.12	−0.40	0.83	0.10	0.77	0.67	0.77	0.17	0.63	0.87	0.54
	0.23	0.65	0.00	0.19	0.01	0.08	0.00	0.68	0.15	0.00	0.73	0.00	0.01	0.00	0.54	0.01	0.00	0.04
Gd	−0.18	−0.04	0.67	0.25	0.61	0.29	0.87	−0.18	−0.51	0.79	0.12	0.69	0.55	0.70	0.05	0.49	0.98	0.69
	0.52	0.90	0.01	0.37	0.02	0.30	0.00	0.52	0.06	0.00	0.68	0.00	0.04	0.00	0.87	0.06	0.00	0.00
Dy	−0.17	−0.05	0.64	0.23	0.59	0.26	0.84	−0.15	−0.50	0.75	0.10	0.66	0.51	0.67	0.03	0.47	1.00	0.73
	0.55	0.86	0.01	0.42	0.02	0.34	0.00	0.59	0.06	0.00	0.72	0.01	0.05	0.01	0.93	0.08	0.00	0.00
Yb	−0.12	−0.08	0.52	0.16	0.51	0.19	0.70	−0.08	−0.44	0.65	0.10	0.54	0.39	0.57	−0.02	0.36	0.97	0.79
	0.67	0.79	0.05	0.57	0.05	0.51	0.00	0.77	0.10	0.01	0.73	0.04	0.15	0.03	0.95	0.19	0.00	0.00
Lu	−0.27	0.08	0.64	0.27	0.56	0.36	0.75	−0.03	−0.35	0.74	0.09	0.64	0.53	0.69	0.11	0.47	0.94	0.76
	0.33	0.77	0.01	0.32	0.03	0.18	0.00	0.92	0.21	0.00	0.76	0.01	0.04	0.00	0.69	0.08	0.00	0.00

Table 5b (*continued*)

Nb	Cs	Ba	Hf	Pb	Th	U	La	Ce	Nd	S	Eu	Gd	Dy	Yb	Lu
0.21	0.92	1.00													
0.46	0.00														
0.30	−0.15	−0.25	1.00												
0.29	0.59	0.37													
−0.42	0.63	0.47	−0.08	1.00											
0.12	0.01	0.08	0.79												
−0.15	−0.39	**−0.60**	0.69	−0.06	1.00										
0.60	0.15	0.02	0.00	0.85											
−0.08	0.00	−0.14	0.80	0.15	0.81	1.00									
0.79	1.00	0.63	0.00	0.59	0.00										
−0.21	−0.39	**−0.62**	0.52	−0.09	0.97	0.70	1.00								
0.46	0.15	0.01	0.05	0.76	0.00	0.00									
−0.20	−0.38	**−0.61**	0.55	−0.08	0.98	0.73	1.00	1.00							
0.49	0.16	0.02	0.03	0.77	0.00	0.00	0.00								
−0.20	−0.36	**−0.57**	0.58	−0.07	0.98	0.77	0.99	1.00	1.00						
0.47	0.18	0.03	0.02	0.81	0.00	0.00	0.00	0.00							
−0.16	−0.34	**−0.53**	0.65	−0.08	0.99	0.83	0.97	0.98	0.99	1.00					
0.58	0.21	0.04	0.01	0.79	0.00	0.00	0.00	0.00	0.00						
−0.20	−0.24	−0.35	0.54	−0.01	0.86	0.86	0.84	0.86	0.89	0.91	1.00				
0.48	0.39	0.20	0.04	0.97	0.00	0.00	0.00	0.00	0.00	0.00					
−0.10	−0.31	−0.49	0.69	−0.10	0.97	0.87	0.95	0.96	0.97	0.99	0.93	1.00			
0.72	0.27	0.07	0.01	0.72	0.00	0.00	0.00	0.00	0.00	0.00	0.00				
0.02	−0.31	−0.48	0.73	−0.15	0.95	0.84	0.92	0.93	0.95	0.97	0.89	0.99	1.00		
0.94	0.26	0.07	0.00	0.59	0.00	0.00	0.00	0.00	0.00	0.00	0.00	0.00			
0.25	−0.29	−0.45	0.80	−0.22	0.87	0.75	0.81	0.82	0.83	0.86	0.74	0.89	0.95	1.00	
0.38	0.30	0.10	0.00	0.42	0.00	0.00	0.00	0.00	0.00	0.00	0.00	0.00	0.00		
0.21	−0.22	−0.33	0.77	−0.13	0.83	0.83	0.76	0.77	0.79	0.84	0.85	0.89	0.94	0.94	1.00
0.46	0.43	0.23	0.00	0.64	0.00	0.00	0.00	0.00	0.00	0.00	0.00	0.00	0.00	0.00	

$(Eu/Eu^*)_N$ <0.85. This indicates that the studied sediments have been derived from a highly differentiated source (Taylor and McLennan, 1985).

The BJR sediment samples show uniform K/Rb ratios and that plot close to a typical differentiated magmatic suite defined by a major trend with K/Rb ratio of 230 (Fig. 17; Shaw, 1968). The phenomenon evaluated from the studied samples demonstrates the chemically coherent nature of the sediments and derivation from rocks of acidic and intermediate compositions. Ferromagnesian trace elements such as Cr, Ni, Co and V illustrate usually analogous behavior in magmatic processes, but they may be fractionated during weathering (Feng and Kerrich, 1990). In both sample groups in this study (i.e., bar-top and sedimentary facies sediments), Cr is slightly enriched with respect to the average composition of the UCC (Fig. 9), and this may imply some contribution from basic to ultrabasic rocks in the source terrain. Elevated values of Cr (>150 ppm) and Ni (>100 ppm) and Cr/Ni ratios of 1.3–1.5 are diagnostic of ultrabasic rocks (Garver et al., 1996). However, in the analyzed sediments, Cr concentrations range from 20 to 80 ppm (mean 48 ppm) and Ni concentrations are mostly below the detection limit of 20 ppm (Table 3). Therefore, derivation of the studied sediment samples from basic/ultrabasic rocks is quite unlikely.

4.5. Weathering in the source area

Values of CIA for the BJR sediment samples vary from 51 to 62 with an average of 53, indicating that the studied sediment samples were derived from partially weathered materials (Table 2). The CIA values of the fine sand bar-top samples range from 51 to 54, whereas those in the fine sand, silt and mud facies samples, ranges from 50 to 62. This indicates increasing weathering or alteration intensity from upstream to downstream of the BJR. The mean CIA value for the BJR sediment samples is similar to that of the UCC (50). The CIA values for the BJR sediment samples are quite similar to those of the Ganges River sediments (48–55) in the southwestern Himalayas (Singh, 2010) but they are more similar to those of the Yamuna River System sediments in the Himalaya (~51 to 69; average ~60) (Dalai et al., 2002). Fig. 18 shows the plot of the CIA values for the BJR sediment samples in the Al_2O_3–$(CaO^* + Na_2O)$–K_2O (A–CN–K) diagram showing the potential parent source rocks from the Higher and Lesser Himalayas, according to the study of Singh (2010). The analyzed sediment samples plot near the plagioclase–K-feldspar join line, mostly within the HHSC field and close to UCC plot. This demonstrates low to moderate chemical weathering of the source rock (Fig. 18).

Fractionation of Ce is known to occur during weathering and sedimentary processes (Borges et al., 2008). In the early stages, negative Ce anomalies are observed in weathering products like secondary hydrous phosphates (Braun et al., 1998), and positive Ce anomalies appear in intensely weathered lateritic profiles where soluble Ce^{3+} oxidizes to insoluble, thermodynamically stable Ce^{4+} and accumulates in secondary cerianite, $Ce(IV)O_2$ (Braun et al., 1998; Pan and Stauffer, 2000). The homogeneous and relatively low Ce anomaly of the BJR sediment samples ($Ce/Ce^* = 0.94–0.99$; Table 3) suggests that the chemical weathering they experienced by the sediments was not intensive. In sedimentary rocks, Th/U is of particular attention, as weathering and recycling characteristically result in loss of U, leading to an elevation in the Th/U ratio. The Th/U ratio in most upper crustal rocks is typically between 3.5 and 4.0 (McLennan et al., 1993). In sedimentary rocks, Th/U values greater than 4.0 may indicate intense weathering in source areas or sediment recycling. The Th/U ratios of the BJR sediment samples range from 3.17 to 6.45, with an average of 5.52 suggesting their derivation from rocks that were formed due to recycling of the crust. A Th/U versus Th plot for the BJR sediment samples (Fig. 19a) shows a characteristic distribution akin to the mean values of fine-grained sedimentary rocks (very fine sand, silt and mud) reported by Taylor and McLennan (1985) and shows the normal weathering trend (McLennan et al., 1993). In addition, sedimentary sorting and recycling can be observed by a plot of Th/Sc versus Zr/Sc (McLennan et al., 1993) (Fig. 19b). First-order sediments demonstrate a simple positive correlation between these ratios, whereas recycled sediments show a substantial increase in Zr/Sc with far less increase in Th/Sc. The trend of raised Zr/Sc and nearly constant Th/Sc can also be attributed to the first-cycle sediments if they originated from largely plutonic sources, as

illustrated by Rahman and Suzuki (2007) in the case of the Miocene sediments of Surma Group in BB. In Th/Sc versus Zr/Sc diagram, the plots of the BJR sediment samples follow a general trend consistent with their direct derivation from granitoid rocks (Fig. 19b). Ratios of Rb/Sr in sediments also reflect the degree of the source-rock weathering (McLennan et al., 1993). The Miocene Surma Group sandstones in the BB have an average Rb/Sr ratio of 0.62, which is higher than the average Rb/Sr ratio in the UCC (0.32) but lower than the average Rb/Sr

Table 5c
Correlation matrix of the facies and bar-top samples of the Brahmaputra–Jamuna River sediments. Underscores of coefficients indicate significant (+) correlation and (−) correlations are denoted by bolds.

	SiO_2	Al_2O_3	TiO_2	Fe_2O_3	MnO	MgO	CaO	Na_2O	K_2O	P_2O_5	CIA	Be	V	Cr	Co	Br	Y	Zr	Nb	Cs	Ba	Hf
SiO2	1.00																					
Al_2O_3	**−0.95**	1.00																				
	0.00																					
TiO_2	**−0.82**	0.66	1.00																			
	0.00	0.00																				
Fe_2O_3	**−0.95**	0.90	0.86	1.00																		
	0.00	0.00	0.00																			
MnO	**−0.71**	0.59	0.87	0.84	1.00																	
	0.00	0.00	0.00	0.00																		
MgO	**−0.96**	0.88	0.85	0.89	0.70	1.00																
	0.00	0.00	0.00	0.00	0.00																	
CaO	−0.05	−0.14	0.51	0.07	0.40	0.24	1.00															
	0.80	0.47	0.00	0.73	0.03	0.20																
Na_2O	0.38	−0.28	−0.34	−0.54	−0.54	−0.30	0.22	1.00														
	0.04	0.14	0.07	0.00	0.00	0.11	0.24															
K_2O	**−0.62**	0.77	0.15	0.59	0.21	0.44	−0.66	−0.30	1.00													
	0.00	0.00	0.42	0.00	0.27	0.02	0.00	0.11														
P_2O_5	−0.47	0.32	0.79	0.55	0.67	0.53	0.67	−0.09	−0.10	1.00												
	0.01	0.08	0.00	0.00	0.00	0.00	0.00	0.63	0.60													
CIA	0.06	−0.01	−0.04	−0.07	−0.04	−0.02	0.12	0.24	0.05	0.23	1.00											
	0.76	0.96	0.84	0.70	0.83	0.91	0.54	0.21	0.80	0.23												
Be	**−0.73**	0.59	0.94	0.80	0.90	0.80	0.62	−0.33	0.07	0.80	0.03	1.00										
	0.00	0.00	0.00	0.00	0.00	0.00	0.00	0.07	0.71	0.00	0.99											
V	**−0.90**	0.76	0.97	0.93	0.87	0.92	0.39	−0.44	0.30	0.70	−0.05	0.92	1.00									
	0.00	0.00	0.00	0.00	0.00	0.00	0.03	0.02	0.11	0.00	0.78	0.00										
Cr	**−0.78**	0.61	0.95	0.80	0.83	0.81	0.50	−0.31	0.13	0.76	0.02	0.89	0.93	1.00								
	0.00	0.00	0.00	0.00	0.00	0.00	0.01	0.09	0.51	0.00	0.94	0.00	0.00									
Co	**−0.93**	0.94	0.70	0.95	0.70	0.85	−0.12	−0.47	0.76	0.44	0.03	0.65	0.81	0.66	1.00							
	0.00	0.00	0.00	0.00	0.00	0.00	0.53	0.01	0.00	0.02	0.87	0.00	0.00	0.00								
Br	0.14	−0.23	0.17	−0.21	0.05	0.03	0.81	0.59	−0.56	0.37	0.20	0.25	0.08	0.19	−0.29	1.00						
	0.47	0.23	0.38	0.28	0.79	0.89	0.00	0.00	0.00	0.05	0.28	0.18	0.69	0.32	0.12							
Y	−0.18	−0.03	0.66	0.27	0.61	0.30	0.80	−0.10	−0.49	0.73	0.00	0.70	0.52	0.65	0.05	0.42	1.00					
	0.33	0.89	0.00	0.16	0.00	0.11	0.00	0.60	0.01	0.00	1.00	0.00	0.00	0.00	0.78	0.02						
Zr	−0.27	0.07	0.59	0.30	0.38	0.27	0.38	−0.12	−0.24	0.55	−0.16	0.46	0.45	0.61	0.10	0.03	0.72	1.00				
	0.15	0.71	0.00	0.11	0.04	0.15	0.04	0.54	0.20	0.00	0.40	0.01	0.01	0.00	0.60	0.87	0.00					
Nb	−0.32	0.27	0.14	0.22	0.07	0.25	−0.29	−0.22	0.26	−0.23	−0.21	0.02	0.17	0.18	0.18	−0.41	0.07	0.41	1.00			
	0.09	0.15	0.46	0.24	0.71	0.19	0.12	0.25	0.17	0.22	0.26	0.93	0.38	0.35	0.34	0.03	0.70	0.02				
Cs	**−0.66**	0.78	0.32	0.73	0.45	0.48	−0.54	−0.50	0.92	0.11	−0.03	0.27	0.45	0.26	0.84	−0.59	−0.29	−0.11	0.18	1.00		
	0.00	0.00	0.08	0.00	0.01	0.01	0.00	0.01	0.00	0.58	0.88	0.14	0.01	0.16	0.00	0.00	0.12	0.58	0.34			
Ba	**−0.71**	0.83	0.25	0.66	0.26	0.54	−0.64	−0.37	0.96	−0.12	−0.10	0.12	0.40	0.21	0.78	−0.57	−0.46	−0.15	0.35	0.89	1.00	
	0.00	0.00	0.19	0.00	0.17	0.00	0.00	0.05	0.00	0.51	0.59	0.53	0.03	0.26	0.00	0.00	0.01	0.42	0.06	0.00		

	SiO_2	Al_2O_3	TiO_2	Fe_2O_3	MnO	MgO	CaO	Na_2O	K_2O	P_2O_5	CIA	Be	V	Cr	Co	Br	Y	Zr
Hf	−0.24	0.05	0.58	0.27	0.39	0.23	0.43	−0.03	−0.26	0.60	−0.11	0.47	0.43	0.60	0.08	0.13	0.75	0.99
	0.21	0.81	0.00	0.16	0.04	0.21	0.02	0.87	0.17	0.00	0.56	0.01	0.02	0.00	0.69	0.51	0.00	0.00
Pb	−0.03	0.15	0.01	0.16	0.15	−0.07	−0.15	−0.04	0.37	0.29	0.20	0.02	0.03	−0.02	0.27	0.03	−0.18	−0.28
	0.86	0.42	0.97	0.40	0.42	0.70	0.45	0.82	0.05	0.12	0.30	0.92	0.89	0.90	0.15	0.87	0.34	0.13
Th	−0.05	−0.18	0.59	0.18	0.54	0.15	0.77	−0.18	−0.58	0.68	−0.07	0.60	0.45	0.58	−0.05	0.39	0.93	0.71
	0.79	0.34	0.00	0.35	0.00	0.44	0.00	0.34	0.00	0.00	0.73	0.00	0.01	0.00	0.78	0.03	0.00	0.00
U	−0.49	0.28	0.84	0.56	0.65	0.54	0.54	−0.32	−0.14	0.75	−0.11	0.74	0.75	0.79	0.36	0.14	0.79	0.83
	0.01	0.14	0.00	0.00	0.00	0.00	0.00	0.09	0.45	0.00	0.56	0.00	0.00	0.00	0.05	0.45	0.00	0.00
La	−0.08	−0.17	0.56	0.21	0.58	0.17	0.69	−0.38	−0.55	0.55	−0.18	0.58	0.46	0.56	−0.02	0.25	0.86	0.62
	0.67	0.38	0.00	0.26	0.00	0.37	0.00	0.04	0.00	0.00	0.33	0.00	0.01	0.00	0.91	0.18	0.00	0.00
Ce	−0.08	−0.16	0.58	0.21	0.59	0.18	0.73	−0.33	−0.56	0.59	−0.16	0.61	0.47	0.58	−0.02	0.30	0.88	0.63
	0.67	0.39	0.00	0.26	0.00	0.35	0.00	0.07	0.00	0.00	0.41	0.00	0.01	0.00	0.90	0.11	0.00	0.00
Nd	−0.13	−0.12	0.63	0.25	0.61	0.22	0.76	−0.30	−0.55	0.65	−0.12	0.65	0.51	0.62	0.01	0.34	0.90	0.65
	0.51	0.52	0.00	0.19	0.00	0.24	0.00	0.11	0.00	0.00	0.52	0.00	0.00	0.00	0.95	0.06	0.00	0.00
S	−0.21	−0.05	0.68	0.31	0.62	0.30	0.73	−0.32	−0.49	0.67	−0.14	0.68	0.58	0.69	0.08	0.30	0.90	0.72
	0.27	0.81	0.00	0.09	0.00	0.11	0.00	0.09	0.01	0.00	0.46	0.00	0.00	0.00	0.68	0.11	0.00	0.00
Eu	−0.32	0.12	0.76	0.38	0.65	0.46	0.86	−0.10	−0.41	0.81	−0.01	0.79	0.65	0.75	0.18	0.54	0.88	0.56
	0.09	0.55	0.00	0.04	0.00	0.01	0.00	0.61	0.03	0.00	0.94	0.00	0.00	0.00	0.33	0.00	0.00	0.00
Gd	−0.22	−0.01	0.71	0.31	0.64	0.33	0.81	−0.19	−0.50	0.77	−0.05	0.73	0.58	0.71	0.10	0.40	0.96	0.71
	0.25	0.94	0.00	0.09	0.00	0.07	0.00	0.30	0.01	0.00	0.81	0.00	0.00	0.00	0.61	0.03	0.00	0.00
Dy	−0.25	0.01	0.69	0.33	0.63	0.34	0.72	−0.26	−0.45	0.69	−0.11	0.69	0.58	0.70	0.10	0.30	0.96	0.77
	0.19	0.98	0.00	0.08	0.00	0.06	0.00	0.18	0.01	0.00	0.56	0.00	0.00	0.00	0.59	0.11	0.00	0.00
Yb	−0.22	−0.01	0.60	0.28	0.56	0.28	0.59	−0.24	−0.41	0.56	−0.17	0.58	0.49	0.62	0.06	0.18	0.91	0.83
	0.25	0.95	0.00	0.14	0.00	0.13	0.00	0.20	0.03	0.00	0.36	0.00	0.01	0.00	0.76	0.33	0.00	0.00
Lu	−0.34	0.12	0.69	0.36	0.59	0.43	0.64	−0.18	−0.32	0.65	−0.15	0.66	0.59	0.71	0.16	0.28	0.90	0.80
	0.07	0.53	0.00	0.05	0.00	0.02	0.00	0.34	0.08	0.00	0.45	0.00	0.00	0.00	0.40	0.13	0.00	0.00

Table 5c (*continued*)

Nb	Cs	Ba	Hf	Pb	Th	U	La	Ce	Nd	S	Eu	Gd	Dy	Yb	Lu
0.34	−0.12	−0.20	1.00												
0.06	0.53	0.29													
−0.56	0.47	0.23	−0.20	1.00											
0.00	0.01	0.22	0.30												
−0.03	−0.34	−0.53	0.73	−0.13	1.00										
0.87	0.06	0.00	0.00	0.50											
0.18	0.04	−0.05	0.81	−0.10	0.82	1.00									
0.34	0.82	0.78	0.00	0.60	0.00										
0.04	−0.32	−0.47	0.60	−0.24	0.94	0.76	1.00								
0.85	0.09	0.01	0.00	0.21	0.00	0.00									
0.01	−0.32	−0.49	0.63	−0.21	0.96	0.77	1.00	1.00							
0.96	0.08	0.01	0.00	0.27	0.00	0.00	0.00								
−0.02	−0.31	−0.48	0.65	−0.18	0.97	0.80	0.99	1.00	1.00						
0.93	0.09	0.01	0.00	0.34	0.00	0.00	0.00	0.00							
0.07	−0.27	−0.41	0.71	−0.22	0.96	0.85	0.98	0.98	0.99	1.00					
0.72	0.15	0.03	0.00	0.25	0.00	0.00	0.00	0.00	0.00						
−0.13	−0.23	−0.36	0.59	−0.03	0.87	0.80	0.81	0.84	0.88	0.89	1.00				
0.51	0.23	0.05	0.00	0.86	0.00	0.00	0.00	0.00	0.00	0.00					
0.00	−0.27	−0.44	0.73	−0.15	0.97	0.85	0.93	0.95	0.97	0.97	0.94	1.00			
0.99	0.14	0.01	0.00	0.43	0.00	0.00	0.00	0.00	0.00	0.00	0.00				
0.17	−0.25	−0.38	0.77	−0.25	0.94	0.85	0.93	0.94	0.95	0.97	0.88	0.98	1.00		
0.37	0.18	0.04	0.00	0.19	0.00	0.00	0.00	0.00	0.00	0.00	0.00	0.00			
0.36	−0.23	−0.32	0.82	−0.34	0.85	0.78	0.84	0.85	0.84	0.88	0.73	0.88	0.95	1.00	
0.05	0.22	0.08	0.00	0.07	0.00	0.00	0.00	0.00	0.00	0.00	0.00	0.00	0.00		
0.31	−0.18	−0.24	0.80	−0.25	0.83	0.83	0.80	0.81	0.82	0.86	0.83	0.88	0.94	0.95	1.00
0.09	0.35	0.20	0.00	0.18	0.00	0.00	0.00	0.00	0.00	0.00	0.00	0.00	0.00	0.00	

ratio in post-Archean Australian shales (0.80; McLennan and Taylor, 1983). The values of Rb/Sr in the bar-top sediments (fine-sand samples) are in the 0.42–0.71 range with a mean of 0.53, whereas those in the facies samples (fine sand, silt and mud samples) are in the 0.39–1.71 range with a mean of 0.70. Despite compositional variations among the fine sand, silt and mud facies samples, Rb/Sr values in all the BJR sediment samples (Table 4) suggest minor to moderate weathering in their source area. This finding is similar to the finding for the Miocene Surma Group sediments of BB as discussed by Rahman and Suzuki (2007).

5. Discussion

The chemical composition of clastic sediments is the ultimate product of various geological factors. These factors comprise, among others, source-rock composition, intensity of weathering (both physical and chemical), rate of sediment supply, sorting (both textural and mineralogical) during transportation and deposition, and finally post-depositional weathering (Roddaz et al., 2006 and reference therein). Each of these factors needs to be evaluated prior to drawing conclusions on the nature of source rocks (provenance of sediments) tectonics and source weathering of the region as inferred from the chemistry of clastic sediments.

The present study demonstrates that grain sizes of sediments influence variations in chemical compositions of sediments in the BJR. Separation of sand from mud by fluvial processes operating in the BJR system resulted in considerable variations in concentrations of many elements (TiO_2, Fe_2O_3T, CaO, K_2O, P_2O_3, MnO, Na_2O, Rb, Zr, Sr, Ba, Nb, and Th) with respect to SiO_2/Al_2O_3, reflecting contrast in geochemistry of the samples with respect to grain size (Figs. 8, 10 and 11). However, CaO, Na_2O and Sr increase with increasing grain size as implied in Figs. 8 and 11 indicating further control by feldspar content on chemical composition of sediments. In addition, Pb showsa slight decrease as SiO_2/Al_2O_3 increases and lower Pb values are found in fine-grained particles (very fine sand, silt and mud), suggesting that Pb is

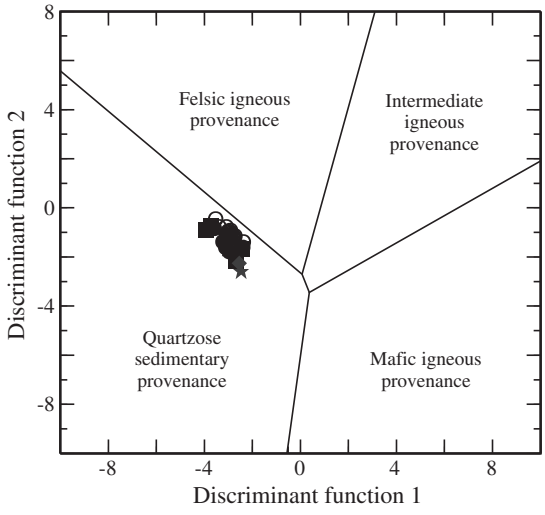

Fig. 13. Classification plot of discriminant functions F1 and F2 for the Brahmaputra–Jamuna River sediments. Provenance fields are from Roser and Korsch (1988). Legends of plot symbols are shown in Fig. 6.

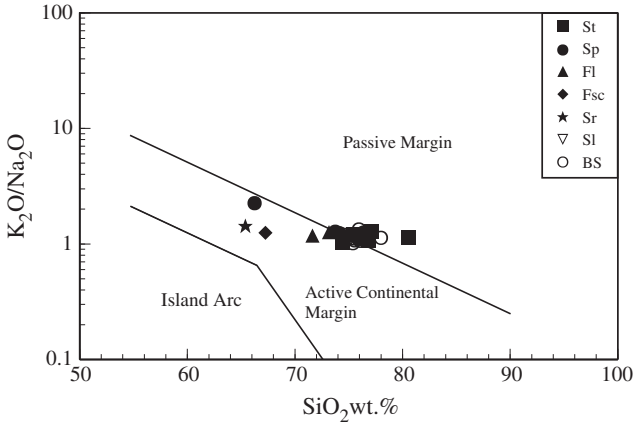

Fig. 14. Tectonic discrimination diagram for the Brahmaputra–Jamuna River sediments. Boundaries of fields are from Roser and Korsch (1986).

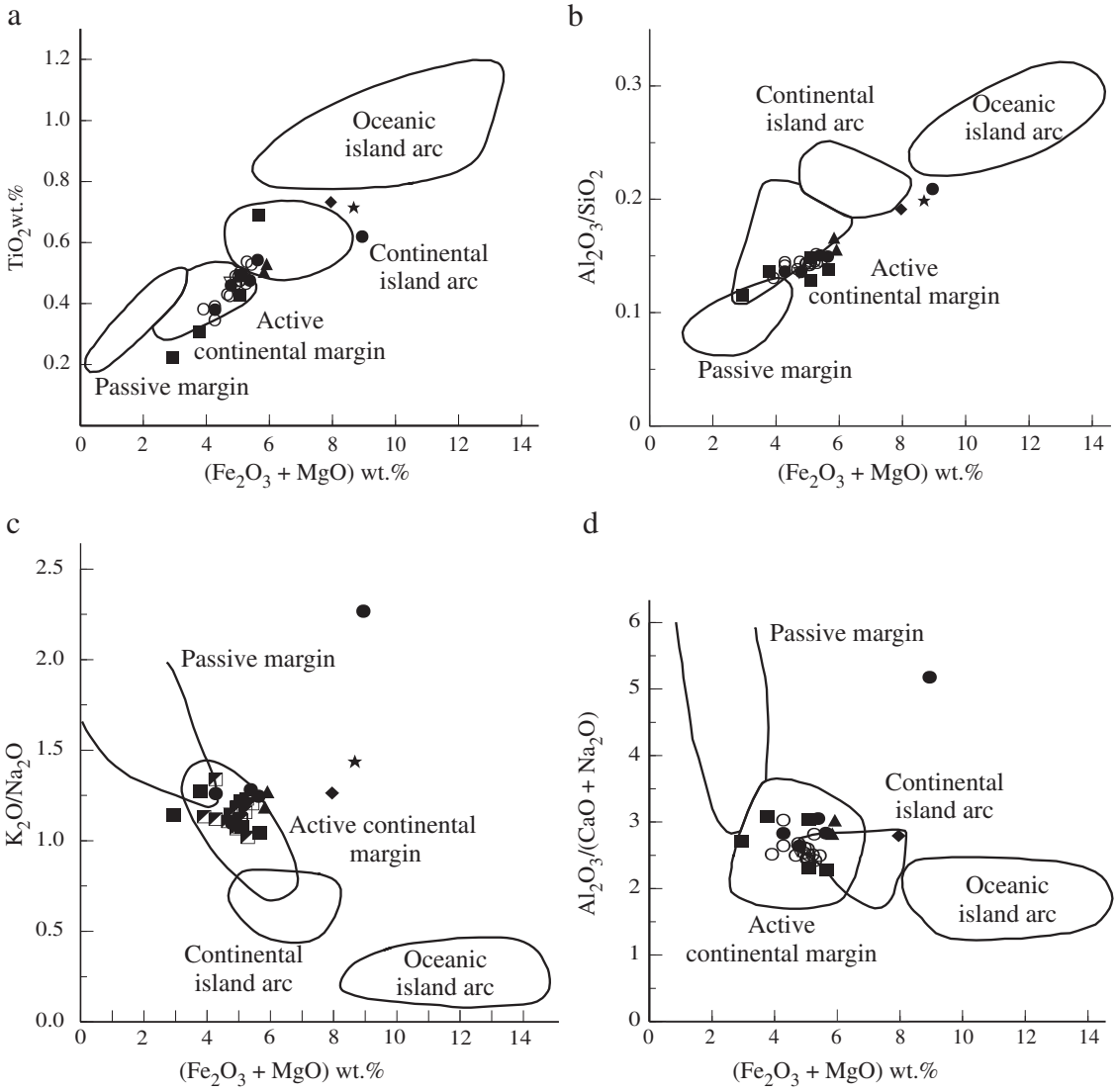

Fig. 15. Tectonic-setting discrimination diagrams for the Brahmaputra–Jamuna River sediments. Boundaries of fields are from Bhatia (1983). Legends of plot symbols are shown in Fig. 6.

derived from both feldspars and clay-sized detritus. Poor correlation of Ba with grain size is probably due to the compensation effect produced by its residence in both feldspar and clay. Decrease in Zr abundance with respect to variations in SiO_2/Al_2O_3 is characteristic of zircon concentration. Sporadic high values and/or broad ranges of several other elements (Ce, Th, Y, Ni, and Cr) suggest contributions from heavy minerals.

The Eu anomaly is generally regarded as inherited from the sediment sources (McLennan et al., 1993 and references therein). Weak Eu anomalies are usually ascribed to input of basic detritus whereas strong Eu anomalies are related to felsic source (Cullers, 2000). In the Eu/Eu* versus GdN/YbN diagram (Fig. 16), most of the sediments of BJR have GdN/YbN lower than 2.0 and Eu anomaly lower than 0.85, which are characteristic of PAAS-like sediments.

Sands are more likely to be affected by mineral sorting (McLennan, 1989) than fine-grained sedimentary rocks like shales. This would be reflected in the REE patterns of the sandstones (Fig. 12). Sands analyzed in this study differ in grain size from medium to very fine-grained. Nevertheless, all the sands show similar REE patterns, indicating that the heavy mineral sorting, affected all samples almost in a similar manner, regardless of their grain size. In spite of little differing REE contents, the sand and mud samples have similar REE patterns (Fig. 12).

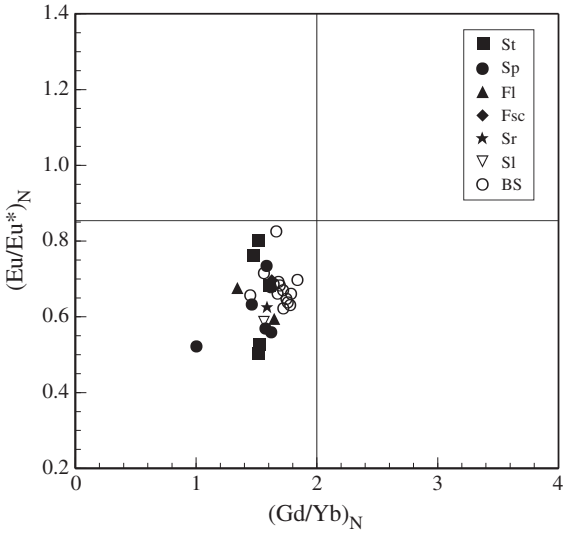

Fig. 16. Plot of Eu/Eu* vs. $(Gd/Yb)_N$ for the Brahmaputra–Jamuna River sediments. All the sediments are significantly depleted in Eu (i.e., low Eu/Eu* values) indicating that the sediments have been derived from a highly differentiated source (Taylor and McLennan, 1985).

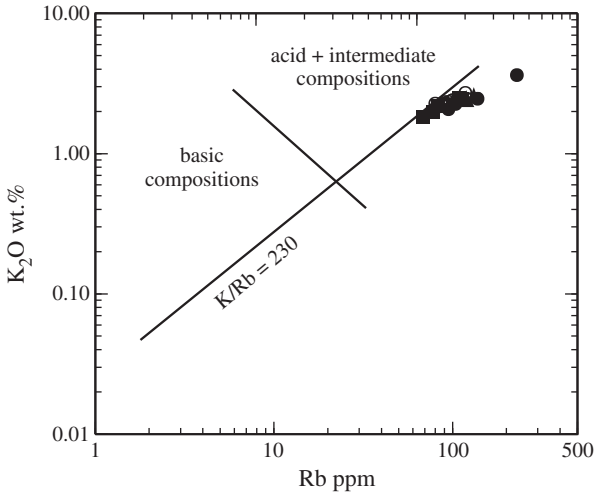

Fig. 17. Distribution of K and Rb in the Brahmaputra–Jamuna River sediments relative to a K/Rb ratio of 230 (= main trend of Shaw, 1968).

This result is in agreement with the study of Miocene sediments in the BB by Rahman and Suzuki (2007) and floodplain deposits of southern India by Singh and Rajamani (2001a). These authors demonstrated that REE as well as Fe, Mg, Mn, Ni and Cr tend to be more concentrated in finer than in coarser particles. They suggested that these enrichments were due to physical fluvial sorting leading to chemical differentiation.

The discriminant diagrams clearly indicate a felsic continental margin source for the BJR sediments (Figs. 13–15), with superimposed maturation resulting from the destruction of labile constituents, particularly feldspar. Passive margin sediments are enriched in SiO_2 because of quartz concentration, and are consequently depleted in most other elements as a result of dilution. The weak but noticeable contrast in chemistry between the bar-top and facies samples based on the major element discriminant plots is related to varying degrees of weathering, sedimentary maturation or diagenesis.

In this study, the values of CIA and plots of A–CN–K (Fig. 18) clearly show that the BJR sediment source was moderately weathered. The relatively linear and spread-out trend the data sets towards illite–muscovite compositions (Fig. 18) is typical of fine particles produced in non-steady state weathering regimes, where active tectonism permits erosion of all levels within soil profiles (Nesbitt et al., 1997). This implies active uplift throughout the source region of the BJR sediments in the Himalayas. The CIA values of the studied samples are analogous to the Miocene sediment of Surma Group in Bengal Basin (Rahman and Suzuki, 2007). Residence time on floodplains has a strong influence in sediment compositions, with longer residence times allowing greater chemical weathering, to the extent that first-cycle quartz arenites can be produced (Johnsson, 1994). In this respect, the low CIA values in the sand-sized bar-top sediments suggest less intense weathering, whereas the moderate CIA values in the very fine-grained silt and mud in the facies samples imply longer residence times and consequently more intense weathering.

6. Conclusions

The bulk geochemistry of clastic sediments from the Brahmaputra–Jamuna River is influenced by grain size, with many elements showing considerable variations with respect to variations in SiO_2/Al_2O_3 in different sedimentary facies sediment samples. Concentrations of TiO_2, Fe_2O_3, MgO, K_2O, P_2O_5, Rb, Nb, Cr, V, Y, Ce, Th and Ga slightly decrease with increasing SiO_2/Al_2O_3 and grain size, suggesting clay matrix control on chemical composition of sediments from the Brahmaputra–Jamuna River. In contrast, concentrations of CaO, Na_2O, Sr and Pb increase with increasing SiO_2/Al_2O_3, and grain size, suggesting residence of these substances in feldspar. Decrease in Zr with respect to increase in grain size is likely due to controls both by clay matrix and heavy minerals. In addition, heavy minerals' sorting also influences Ce, Th, Y and Cr abundances in some of the samples. The fluvial sediments in the Brahmaputra–Jamuna River have dominantly quartzolithic, specifically quartzose composition, even though some samples show feldspathic and quartz arenitic sandstone composition. These sediments are characterized by abundant low-grade metamorphic, sedimentary lithics, low feldspar and low volcanic detritus, which demonstrate that

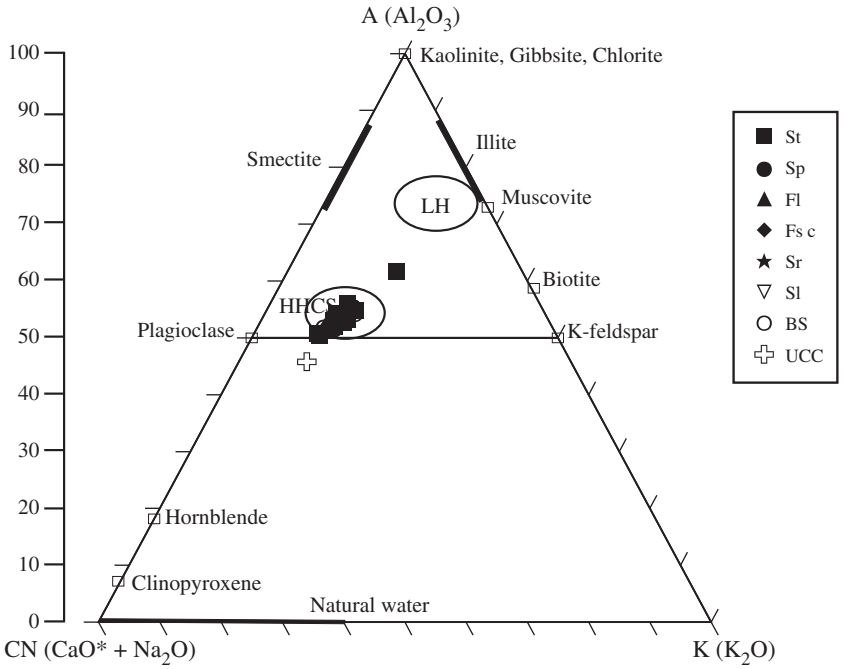

Fig. 18. Plots of A–CN–K with CIA values on the vertical axis (after Nesbitt and Young, 1984, 1989) for the Brahmaputra–Jamuna River sediments. Fields for Higher and Lesser Himalaya source rocks (Singh, 2009) and UCC (Taylor and McLennan, 1985) are also plotted.

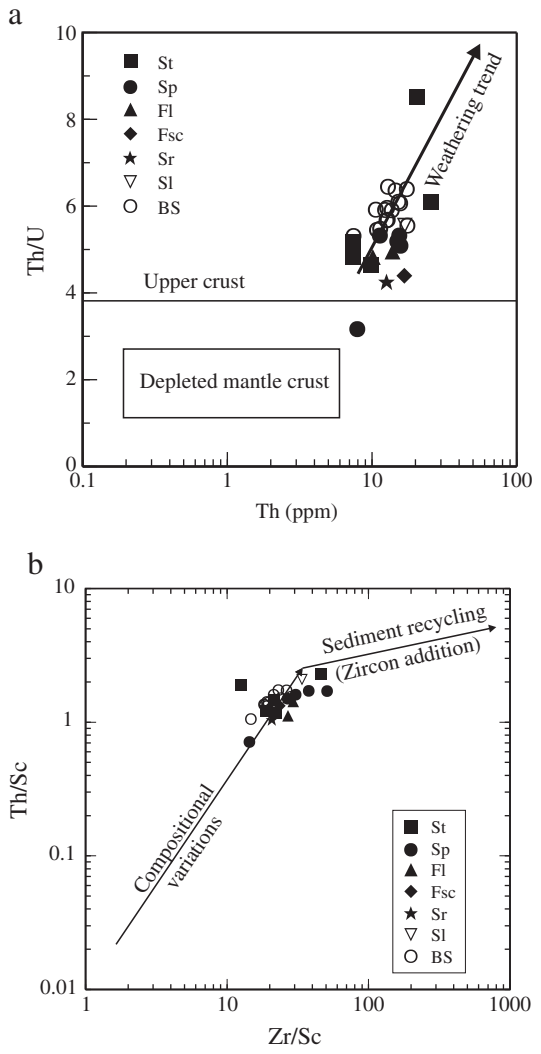

Fig. 19. Plots of (a) Th/U versus Th and (b) Th/Sc versus Zr/Sc for the Brahmaputra–Jamuna River sediments (trends in the plots are from McLennan et al., 1993).

fluvial sediments in the Brahmaputra–Jamuna River originated from a quartzose recycled orogen province. Evidences of tectonic discrimination diagrams suggest that the fluvial sediments in the Brahmaputra–Jamuna River were derived from rocks developed in an active continental margin. Consistency in the REE geochemistry of all the studied samples suggests a high degree of sediment homogenization through several episodes of sedimentary reworking. The low to moderate chemical indices of alteration (51 to 62) of the Brahmaputra–Jamuna fluvial sediments indicate that these sediments were delivered from low to moderately weathered sedimentary source regions, and they experienced a very low degree of chemical weathering after deposition. The geochemical characteristics preserve the signatures of a recycled provenance for the Brahmaputra–Jamuna fluvial sediments in relation to their mineralogy. The present geochemical data suggest that the Brahmaputra–Jamuna fluvial sediments have chemical composition similar to the mean compositions of the Higher Himalaya rocks, indicating that the sediments clearly resemble the upper crust available to erosion in the Himalaya.

Acknowledgements

The work is part of the first author's Ph.D. research, which was benefited by the financial support from the Japanese Government (MONBUKAGAKUSHO Scholarship 2007–2010). The authors also acknowledge the organizers of the *GOLDSCHMIDT 2010: Earth, Energy and Environment* Conference, Knoxville, TN, USA for the opportunity given to us to present our work at the conference and inviting our paper to this special issue of *Geochemical Sampling Media*. Dr. Federico Spagnoli and Dr. John Carranza are gratefully acknowledged for their constructive comments, which significantly improved the manuscript.

References

Armstrong-Altrin, J.S., Verma, S.P., 2005. Critical evaluation of six tectonic setting discrimination diagrams using geochemical data of Neogene sediments from known tectonic settings. Sediment. Geol. 177, 115–129.
Bhatia, M.R., 1983. Plate tectonics and geochemical composition of sandstones. Geology 91, 611–627.
Bhatia, M.R., Crook, K.A.W., 1986. Trace element characteristics of graywackes and tectonic setting discrimination of sedimentary basins. Contrib. Mineral. Petrol. 92, 181–193.
Borges, J.B., Huh, Y., Moon, S., Noh, H., 2008. Provenance and weathering control on river bed sediments of the eastern Tibetan Plateau and the Russian Far East. Chem. Geol. 254, 52–72.
Boruah, S., Gilvear, D., Hunter, P., Sharma, N., 2008. Quantifying channel planform and physical habitat dynamics on a large braided river using satellite data—the Brahmaputra, India. River Res. Appl. 24, 650–660.
Braun, J.-J., Viers, J., Dupré, B., Polve, M., Ndam, J., Muller, J.-P., 1998. Solid/liquid REE fractionation in the lateritic system of Goyoum, East Cameroon: the implication for the present dynamics of the soil covers of the humid tropical regions. Geochim. Cosmochim. Acta 62, 273–299.
Coleman, J.M., 1969. Brahmaputra River: channel processes and sedimentation. Sediment. Geol. 3, 129–239.
Condie, K.C., 1991. Another look at rare earth elements in shales. Geochim. Cosmochim. Acta 55, 2521–2531.
Cullers, R., 1988. Mineralogical and chemical changes of soil and stream sediment formed by intense weathering of Danburg granite, Georgia, U.S.A. Lithos 21, 301–314.
Cullers, R.L., 1994. The controls on the major and trace element variation of shales, siltstones, and sandstones of Pennsylvanian–Permian age from uplifted continental blocks in Colorado to platform sediment in Kansas, USA. Geochim. Cosmochim. Acta 58, 4955–4972.
Cullers, R.L., 2000. The geochemistry of shales, siltstones and sandstones of Pennsylvanian–Permian age, Colorado, USA: implications for provenance and metamorphic studies. Lithos 51, 181–203.
Cullers, R.L., Podkovyrov, V.N., 2000. Geochemistry of the Mesoproterozoic Lakhanda shales in southeastern Yakutia, Russia: implications for mineralogical and provenance control, and recycling. Precambrian Res. 104, 77–93.
Cullers, R.L., Basu, A., Suttner, L.J., 1988. Geochemical signature of provenance in sand-size material in soils and stream sediments near the Tobacco Root batholith, Montana, USA. Chem. Geol. 70, 335–348.
Dalai, T.K., Krishnaswami, S., Sarin, M.M., 2002. Major ion chemistry in the headwaters of the Yamuna river system: chemical weathering, its temperature dependence and CO_2 consumption in the Himalaya. Geochim. Cosmochim. Acta 66, 3397–3416.
Das, B.K., AL-Mikhlafi, A.S., Kaur, P., 2006. Geochemistry of Mansar Lake sediments, Jammu, India: implication for source-area weathering, provenance, and tectonic setting. J. Asian Earth Sci. 26, 649–668.
Dewey, J.F., Bird, J.M., 1970. Mountain belts and new global tectonics. J. Geophys. Res. 40, 695–707.
Dewey, J.F., Cande, S., Pitman, W.C.I., 1989. Tectonic evolution of the India–Eurasia collision zone. Eclogae Geol. Helv. 82, 717–734.
Dickinson, W.R., 1985. Interpreting provenance relations from detrital modes of sandstones. In: Zuffa, G.G. (Ed.), Provenance of Arenites: Advanced Study Institute Series, 148. NATO.
Fairbridge, R.W. (Ed.), 1972. The Encyclopedia of Geochemistry and Environmental Sciences. Van Nostrand Reinhold Company, New York. 1344 pp.
Fedo, C.M., Eriksson, K.A., Krogstad, E.J., 1996. Geochemistry of shales from the Archean (3.0 Ga) Buhwa Greenstone Belt, Zimbabwe: implications for provenance and source-area weathering. Geochim. Cosmochim. Acta 60, 1751–1763.
Feng, R., Kerrich, R., 1990. Geochemistry of fine-grained clastic sediments in the Archean Abitibi greenstone belt, Canada: implications for provenance and tectonic setting. Geochim. Cosmochim. Acta 54, 1061–1081.
Ferguson, R.I., 1963. Understanding braiding processes un gravel-bed rivers: process and unsolved problems. In: Best, J.L., Bristow, C.S. (Eds.), Braided Rivers, Geol. Soc. London Spec. Pub., 175, pp. 73–87.
France-Lanord, C., Derry, L., Michard, A., 1993. Evolution of the Himalaya since Miocene time: isotopic and sedimentologic evidence from Bengal Fan. In: Treolar, P.J., Searles, M. (Eds.), Himalayan Tectonics: Geol. Soc. London Spec. Publ., 74, pp. 603–621.
Galy, A., France-Lanord, C., 2001. Higher erosion rates in the Himalaya: geochemical constraints on riverine fluxes. Geology 29, 23–26.
Garver, J.I., Scott, T.J., 1995. Trace elements in shale as indicators of crustal provenance and terrane accretion in the southern Canadian Cordillera. Geol. Soc. Am. Bull. 107, 440–453.
Garver, J.I., Royce, P.R., Smick, T.A., 1996. Chromium and nickel in shale of the Taconic foreland: a case study for the provenance of fine-grained sediments with an ultramafic source. J. Sediment. Res. 100, 100–106.

Grantham, J.H., Velbel, M.A., 1988. The influence of climate and topography on rockfragment abundance in modern fluvial sands of the southern Blue Ridge Mountains, North Carolina. J. Sediment. Petrol. 58, 219–227.
Harrison, T.M., Copeland, P., KIdd, W.S.F., Yin, A., 1992. Raising Tibet. Science 255, 1663–1670.
Herron, M.M., 1986. Geochemical classification of terrigeneous sands and shales from core or log data. J. Sediment. Petrol. 58, 820–829.
Hodges, K.V., 2000. Tectonics of the Himalaya and southern Tibet from two perspectives. Geol. Soc. Am. Bull. 112, 324–350.
Holail, H.M., Moghazi, A.K.M., 1998. Provenance, tectonic setting and geochemistry of greywackes and siltstones of the Late Precambrian Hammamat Group, Egypt. Sediment. Geol. 116, 227–250.
Ingersoll, R.V., Bullard, T.F., Ford, R.L., Grimm, J.P., Pickle, J.D., Sares, S.W., 1984. The effect of grain size on detrital modes: a test of the Gazzi–Dickinson point counting method. J. Sediment. Petrol. 54, 103–116.
Johnsson, M.J., 1994. The system controlling the composition of clastic sediments. In: Johnsson, M.J., Basu, A. (Eds.), Processes controlling the composition of clastic sediments: Geol. Soc. London Spec. Pub., 284, pp. 1–19.
Maynard, J.B., Valloni, R., Yu, H.S., 1982. Composition of modern deep-sea sands from arc-related basins. Trench-Forearc Geology: sedimentation and Tectonics on Modern and Ancient Active Plate Margins. In: Legget, J.K. (Ed.), Geol. Soc. Am. Spec. Pap., 284, pp. 21–40.
McCann, T., 1998. Sandstone composition and provenance of the Rotliegend of the NE German Basin. Sediment. Geol. 116, 177–198.
McLennan, S.R., 1989. Rare earth element in sedimentary rocks: influences of provenance and sedimentary processes. In: Lipin, B.R., McKay, G.A. (Eds.), Geochemistry and mineralogy of rare earth elements, reviews in mineralogy: Min. Soc. Am., pp. 169–200.
McLennan, S.M., Taylor, S.R., 1983. Geochemical evolution of the Archean shales from South Africa. I. The Swaziland and Pongola supergroups. Precambrian Res. 22, 93–124.
McLennan, S.M., 2001. Relationships between the trace element composition of sedimentary rocks and upper continental crust. Geochem. Geophys. Geosyst. 2 (paper number 2000GC000109).
McLennan, S.M., Hemming, S., McDennial, D.K., Hanson, G.N., 1993. Geochemical approaches to sedimentation, provenance and tectonics. Geol. Soc. Am. Spec. Pap. 284, 21–40.
Miall, A.D., 1976. Paleocurrent and paleohydrologic analysis of some vertical profiles through a Cretaceous braided stream deposit, Bank Island, Artic Canada. Sedimentology 23, 459–483.
Milliman, J.D., Meade, R.H., 1983. World-wide delivery of river sediment to the oceans. J. Geol. 91, 1–21.
Molnar, P., Tapponnier, P., 1975. Cenozoic tectonics of Asia: effects of a continental collision. Science 189, 419–426.
Morgan, J.P., McIntire, W.G., 1959. Quaternary geology of the Bengal Basin, East Pakistan and India. Bull. Geol. Soc. Am. 70, 319–342.
Mukherjee, A., Frya, A.E., Thomas, W.A., 2009. Geomorphic and hydrologic framework and evolution of the Bengal Basin, India and Bangladesh. J. Asian Earth Sci. 34, 227–244.
Nesbitt, H.W., Young, G.M., 1984. Prediction of some weathering trends of plutonic and volcanic rocks based on thermodynamic and kinetic consideration. Geochim. Cosmochim. Acta 48, 1523–1534.
Nesbitt, H.W., Young, G.M., 1989. Formation and diagenesis of weathering profiles. J. Geol. 97, 129–147.
Nesbitt, H.W., Young, G.M., 1996. Petrogenesis of sediments in the absence of chemical weathering: effects of abrasion and sorting on bulk composition and mineralogy. Sedimentology 43, 341–358.
Nesbitt, H.W., Fedo, C.M., Young, G.M., 1997. Quartz and feldspar stability, steady and non-steady-state weathering, and petrogenesis of siliciclastic sands and muds. J. Geol. 105, 173–191.
Pan, Y., Stauffer, M.R., 2000. Cerium anomaly and Th/U fractionation in the 1.85 Ga Flin Flon Paleosol: clues from REE- and U-rich accessory minerals and implications for paleoatmospheric reconstruction. Am. Mineral. 85, 898–911.
Pettijohn, F.J., Potter, P.E., Siever, R., 1995. Sand and sandstones. In: Quade, J., Cater, J.M.L., Ojha, T.P., Adam, J., Harrison, T.M. (Eds.), Late Miocene environmental change in Nepal and the northern Indian subcontinent: stable isotopic evidence from paleosols. GSA Bulletin, 107. Springer, New York, pp. 1381–1397 (12).
Potter, P.E., 1994. Modern sands of South America: composition, provenance and global significance. Geol. Rundsch. 83, 212–232.
Potter, P.E., Huh, Y., Edmond, J.M., 2001. Deep-freeze petrology of Lena River sand, Siberia. Geology 29, 999–1002.
Rahman, M.J.J., Faupl, P., 2003. The composition of the subsurface Neogene shales of the Surma Group from the Sylhet Trough, Bengal Basin, Bangladesh. Sedimentary geology of the Bengal Basin, Bangladesh, in relation to the Asia–Greater India collision and the evolution of the eastern Bay of Bengal. Sediment. Geol. 155, 407–417.
Rahman, M.J.J., Suzuki, S., 2007. Geochemistry of sandstones from the Miocene Surma Group, Bengal Basin, Bangladesh: implications for Provenance, tectonic setting and weathering. Geochem. J. 41, 415–428.
Rahman, M.J.J., Bari, J., Chodhury, K.R., Suzuki, S., 2008. Heavy mineral composition of the Neogene sandstones and beach sands across the Inani–Dakin Nhila area, southeast Bangladesh: implications for provenance. J. Sediment. Soc. Jpn. 67, 3–17.
Roddaz, M., Viers, J., Brusset, S., Baby, P., Boucayrand, C., Herail, G., 2006. Controls on weathering and provenance in the Amazonian foreland basin: insights from major and trace element geochemistry of Neogene Amazonian sediments. Chem. Geol. 226 (1–2), 31–65.
Rollinson, H.R., 1993. Using Geochemical Data: Evaluation Presentation. Interpretation, Longman, England.
Roser, B.P., Korsch, R.J., 1986. Determination of tectonic setting of sandstone-mudstone suites using SiO_2 content and K_2O/Na_2O ratio. J. Geol. 94, 635–650.
Roser, B.P., Korsch, R.J., 1988. Provenance signatures of sandstone–mudstone suites determined using discriminant function analysis of major-element data. Chem. Geol. 67, 119–139.
Roser, B.P., Ishiga, H., Lee, H.K., 2000. Geochemistry and provenance of Cretaceous sediments from the Eusing block, Gyeongsang Basin, Korea. Mem. Geol. Soc. Jpn. 57, 155–170.
Sarin, M.M., Krishnaswami, S., Dilli, K., Somayajulu, B.L.K., Moore, W.S., 1989. Major ion chemistry of the Ganges–Brahmaputra river system: weathering processes and fluxes to the Bay of Bengal. Geochim. Cosmochim. Acta 53, 997–1009.
Shaw, D.M., 1968. A review of K–Rb fractionation trends by covariance analysis. Geochim. Cosmochim. Acta 32, 573–602.
Singh, P., 2009. Major, trace and REE geochemistry of the Ganga River sediments: influence of provenance and sedimentary processes. Chem. Geol. 266, 251–264.
Singh, P., 2010. Geochemistry and provenance of stream sediments of the Ganga River and its major tributaries in the Himalayan region, India. Chem. Geol. 269, 220–236.
Singh, P., Rajamani, V., 2001a. Geochemistry of the Kaveri flood-plain sediments, Southern India. J. Sediment. Res. 71, 50–60.
Singh, P., Rajamani, V., 2001b. REE geochemistry of recent clastic sediments from the Kaveri floodplains, Southern India: implication to source area weathering and sedimentary processes. Geochim. Cosmochim. Acta 65, 3093–3108.
Singh, M., Sharma, M., Tobschall, H.J., 2005. Weathering of the Ganga alluvial plain, northern India: implications from fluvial geochemistry of the Gomati River. Appl. Geochem. 20, 1–21.
Singh, S.K., Kumar, A., France-Lanord, C., 2006. Sr and $^{87}Sr/^{86}Sr$ in waters and sediments of the Brahmaputra river system: Silicate weathering, CO_2 consumption and Sr flux. Chem. Geol. 234, 308–320.
Tapponnier, P., Peltzer, G., Armijo, R., 1986. Geol. Soc. London Spec. Pub. 19, 115–157.
Taylor, S.R., 1965. The application of trace element data to problems in petrology. In: Ahrens, L.H., Press, E., Runcorn, S.K., Urey, H.C. (Eds.), Phys. Chem. Earth, 6, pp. 133–213.
Taylor, S.R., McLennan, S.M., 1985. The Continental Crust: Its Composition and Evolution. Blackwell, Oxford. 312 pp.
Tripathia, J.K., Ghazanfari, P., Rajamania, V., Tandon, S.K., 2007. Geochemistry of sediments of the Ganges alluvial plains: evidence of large-scale sediment recycling. Quarter. Int. 159, 119–130.
Turekian, K.K., Wedepohl, K.H., 1961. Distribution of the elements in some major units of the earth crust. GSA Bulletin 72, 175–192.
Whitemore, G.P., Crook, K.A.W., Johnson, D.P., 2004. Grain size control of mineralogy and geochemistry in modern river sediment, New Guinea collision, Papua Guinea. Sediment. Geol. 171, 129–157.
Wronkiewicz, D.J., Condie, K.C., 1987. Geochemistry of Archean shales from the Witwaterstrand Supergroup, South Africa: source area weathering and provenance. Geochim. Cosmochim. Acta 51, 2401–2416.
Wronkiewicz, D.J., Condie, K.C., 1989. Geochemistry and provenance of sediments from the Pongola Supergroup, South Africa: evidence for a 3.0-Ga-old continental craton. Geochim. Cosmochim Acta 53, 1537–1549.